Chapter 2
Charge Transport and Photogeneration in Organic Semiconductors: Photorefractives and Beyond

Canek Fuentes-Hernandez

Abstract Over the last decade, the science and technology of organic semiconductors has seen tremendous progress. The electrical and optical properties displayed by state-of-the-art organic semiconductors are remarkable in their tolerance to disorder, their ability to display high charge carrier mobility values and bipolar transport, and in that they can be engineered to display optical activity in the spectral range from the visible to the near-infrared. This new breed of organic materials is forcing us to reevaluate preconceived notions on how to optimize charge transport and photogeneration in disordered organic semiconductors. Lessons learned in the development of these remarkable organic semiconductors have rapidly spread across organic optoelectronic device platforms, from organic photovoltaics to organic field-effect transistors to organic light emitting diodes and to organic photodetectors, and thus are expected to provide further inspiration to continue advancing the science and technology of organic photorefractives. The purpose of this chapter is to provide a broad overview of current understanding of charge transport and photogeneration in organic semiconductors, going from crystalline to amorphous solids as well as to provide a brief overview of novel organic photoconductors that may offer significant opportunities to advance the science and technology of organic optoelectronic devices in general and of organic photorefractives in particular.

2.1 Introduction

The year 2015 has been designated by the United Nations as the International Year of Light and Light-based technologies to celebrate and raise awareness of the impact that light sciences and technologies have had, and are poised to have on

C. Fuentes-Hernandez (✉)
Center for Organic Photonics and Electronics (COPE), School of Electrical and Computer Engineering, Georgia Institute of Technology, Atlanta, GA 30332, USA
e-mail: canek@ece.gatech.edu

P.-A. Blanche (ed.), *Photorefractive Organic Materials and Applications*,
Springer Series in Materials Science 240, DOI 10.1007/978-3-319-29334-9_2

humankind. Light, electromagnetic waves, represent a cornerstone of modern science, technology and society. The publication of James Clerk Maxwell's "A Treatise on Electricity and Magnetism" in 1873 marks a landmark for the physical understanding of electromagnetic phenomena in general and of light in particular. The recognition of light as an electromagnetic phenomena and the rise of the concept of field, taking central stage in Maxwell's equations marked a "*change of conception of reality (that) is the most profound and fruitful that physics has experienced since the time of Newton*" (A. Einstein, (1931) in "*James Clerk Maxwell: A Commemorative Volume* 1831–1931"). Following the publication of Maxwell's treatise, two pivotal experiments were reported: (1) Michelson's unsuccessful attempt to detect the luminiferous aether (A. A. Michelson, Am. J. Sci, 122, 120 (1881)) set the stage for a scientific debate that eventually culminated with the development of the theory of special relativity, having as one of its central postulates the invariance of the speed-of-light in free-space regardless of the relative motion of the observers with respect to the light source and (2) Hertz's report of the photoelectric effect (Hertz, H., Annalen der Physik, 267, 983 (1887)), an unexplained phenomena under Maxwell's electromagnetic theory of light, which ultimately led Albert Einstein to propose the quantized nature of electromagnetic fields, a fundamental contribution towards the development of the theory of quantum mechanics. The theories of relativity and quantum mechanics, therefore, trace their origins to these two critical insights into the physical nature of light; its constant velocity and the quantized nature of electromagnetic fields. The profound scientific and technological consequences of these two ideas have shaped and continue to shape the modern world.

The ability to engineer optoelectronic devices that enable control over the emission, propagation, and collection of light is a trademark of the modern world. The electronic revolution of the twentieth century was enabled by profound advancements in the science and technology of inorganic semiconductors which now allow for several billions of transistors to be fabricated in a single computer chip the size of a coin, and has enabled billions of people around the globe to access and share information and ideas using ever shrinking mobile optoelectronic devices. The raise of consumer electronics, and more recently, of wearable electronics heralds a new era as well as reveals a pressing need for a second semiconductor revolution to better fulfill our desire for ubiquitous information. Next generation semiconductor technologies are poised to free optoelectronic devices from current constrains regarding their area, shape, flexibility, and weight, while at the same time, dramatically improving the sustainability of these technologies. Next generation semiconductors have to be produced from earth abundant materials using environmentally friendly and sustainable production methods, and present a low carbon footprint through their entire life cycle, from extraction of raw materials to recycling of discarded consumer products. Organic semiconductors hold the promise of meeting most of these needs.

Over the last decade, the science and technology of organic semiconductors has seen tremendous progress. The electrical and optical properties displayed by state-of-the-art organic semiconductors are remarkable in their tolerance to disorder,

their ability to display bipolar transport, and in the wide spectral range where they can display significant linear or nonlinear optical activity. This new breed of organic materials is forcing us to reevaluate preconceived notions on how to optimize charge transport and photogeneration in disordered organic semiconductors. Lessons learned in the development of these remarkable organic semiconductors have rapidly spread across organic optoelectronic device platforms, from organic photovoltaics (OPV) [1–3] to organic field-effect transistors [4–7] to organic light emitting diodes [8] and to organic photodetectors [9–11], and thus are expected to provide further inspiration to advance the science and technology of organic photorefractives.

Photorefractive materials are complex material systems that must display both photoconductive and electro-optic properties. As such, it is recognized that the photorefractive effect was first observed in an inorganic crystal, $LiNbO_3$, in 1966 [12]. However, it was until 1990, when Sutter et al. [13, 14] reported the first observation of the photorefractive effect in an organic crystal. Soon after, the photorefractive effect was reported in amorphous polymer composites [15], fully functionalized polymers [16], hybrid organic–inorganic polymer composites [17], low-weight molecular glasses [18], and liquid crystals [19], among others. This wide range of material systems highlights the enormous flexibility offered by organic materials for tailoring their optical and electrical properties through synthetic chemistry and material engineering approaches.

The possibility of achieving larger refractive index modulations than those displayed by inorganic photorefractive materials through the use of engineered synthetic chromophores [20–25] and tailored thermal properties [23, 26, 27] fueled the original interest in amorphous photorefractive polymers. Photorefractive polymers having a low glass transition temperature (T_g) rapidly displayed some of the largest steady-state photorefractive nonlinearities reported in the literature through the so-called orientational enhancement effect [28, 29]. Despite tremendous progress on the optimization of the static response of photorefractive polymers, their dynamic response has remained limited to the millisecond temporal range under cw illumination [23, 26], and around a few hundreds of microsecond under intense nanosecond-pulse illumination [30]. Limitations to the dynamic response find their origin on the orientational dynamics of chromophores dispersed in a low-T_g host, on the small mobility values displayed by amorphous molecular systems having high degree of energetic and positional disorder, and on the poor control over the trap density and distribution in the solid. This is in part because complex tradeoffs exist between establishing the conditions for efficient photogeneration and transport of carriers, and the need for having a large density of strong and mobile dipolar moieties in materials where electrostatic interactions are poorly screened by the surrounding dielectric media. Despite challenges, the lure of real time holography [31, 32] will continue to fuel interest in this class of materials and their applications, ranging from holographic displays, medical imaging, image and signal processing, and optical computing.

The purpose of this chapter is to provide a broad overview of current understanding of charge transport and photogeneration in organic semiconductors, going

from crystalline solids to amorphous solids, and to describe how current-state-of-the-art materials challenge existing descriptions and present significant opportunities to advance the science and technology of organic optoelectronic devices in general and of organic photorefractives in particular.

2.2 Basic Properties of Organic Semiconductors

Organic semiconductors are carbon-based molecular materials held together by weak interactions, such as van der Waals forces or hydrogen bonds [33]. Van der Waals bonds arise from charge fluctuations in molecules. This fluctuations induce dipole moments that create short-range attractive forces ($\propto r^{-6}$) between molecules [34]. The bonding strength is dependent on the polarizability of molecules and is typically on the order of ca. 0.1 eV, at least one order of magnitude weaker than the typical binding energy for covalently bonded crystals such as C in diamond, displaying binding energy values ca. 7.3 eV. Hydrogen bonds involve a hydrogen atom bound to two other atoms with binding energy values of the same order of magnitude as van der Waals forces. These weak interactions in organic semiconductors leave electronic states of isolated molecules in the bulk of a solid relatively unchanged. The properties of organic molecules in the bulk are nonetheless highly sensitive to molecular packing and electrostatic environment. The presence of charge carriers or dipolar moieties in an organic semiconductor leads to local polarization fields and to conformational and energetic disorder which are critical in determining the electrical and optical properties of the bulk. In general, it must be borne in mind that the bulk properties of organic semiconductors can seldom be derived exclusively from the properties of isolated neutral molecules as they reflect complex molecular interactions existing in the solid. To understand the implications that these characteristics have on the photogeneration, transport, and trapping of charge carriers in organic photoconductors, in this section we will provide an overview of some important electronic properties of organic semiconductors.

2.2.1 Organic Molecules

The optical and electrical properties of organic molecules are closely related to the existence of delocalized π-electrons. In organic molecules of interest, electrons in carbon atoms form either strong covalent bonds, sigma(σ)-bonds resulting from head-on overlapping of two carbon's sp^2 hybridized orbitals, or weak covalent bonds, pi(π)-bonds, resulting from off-plane p_z orbital overlap.

Within the framework of molecular orbital theory, each covalent bond is represented as the linear superposition of the wave function of each electron associated with a given interacting orbital. As an example, in a simple ethylene

molecule, C_2H_4, the π-bond between two carbon atoms results from the linear superposition of the wave functions of two π-electrons occupying p_z orbitals in each carbon atom, represented by $|\psi_1^{p_z}\rangle$ and $|\psi_2^{p_z}\rangle$, respectively, leading to the formation of two possible states: a low energy state $|\pi\rangle \propto |\psi_1^{p_z}\rangle + |\psi_2^{p_z}\rangle$, displaying a high probability for finding an electron between the two carbon nuclei, therefore called a bonding state; and a high energy state $|\pi^*\rangle \propto |\psi_1^{p_z}\rangle - |\psi_2^{p_z}\rangle$, displaying a low probability for finding an electron between the atoms nuclei, and consequently called antibonding state. The states $|\pi\rangle$ and $|\pi^*\rangle$ are the highest occupied molecular orbital (HOMO) and lowest occupied molecular orbital (LUMO), respectively.

Organic molecules of interest for optoelectronic applications display alternate σ and π bonds that form extended chains (conjugate bridges) or rings (aromatic groups). The formation of such alternate-bond structures leads to π-electrons that are highly delocalized. Small molecules, oligomers, or polymers presenting this type of alternation are known as conjugated. In conjugated molecules, the HOMO and LUMO are typically related, but not exclusively, to $|\pi\rangle$ and $|\pi^*\rangle$ states [35].

The electronic and optical properties of organic molecules are theoretically derived through molecular orbital calculations that use wave function methods (e.g. Hartree–Fock method), density functional theory, or that combine both approaches. These types of calculations are aimed at solving the static Schrödinger equation by finding a set of molecular orbitals $|\psi_n\rangle$ and energy eigenvalues $E_n = \hbar\omega_n$, where $\omega_n = 2\pi\nu_n$ and $\hbar = h/2\pi$ is the reduced Planck's constant, from which the HOMO and LUMO energies are determined. Similar methods are also used to rationalize the electronic and geometric structures, redox properties and electronic excitations and packing of large molecular assemblies, oligomers or polymers, albeit at increasing computational costs [35, 36].

At the *molecular level*, the energy difference between the one-electron molecular orbitals defined by the HOMO and LUMO, known as the HOMO–LUMO gap ($E_{\text{HOMO–LUMO}}$), is in general *not equal* to experimentally measured energy gaps such as the fundamental gap or optical gap [37]. The fundamental gap is defined as $E_{\text{fund}} = \text{IE} - \text{EA}$, where IE represents the ionization energy (also referred to as the ionization potential) and EA the electron affinity of a molecule in the gas phase. The IE corresponds to the energy difference between the $N-1$ electron and N-electron states, experimentally measured by gas-phase ultraviolet photoelectron spectroscopy (UPS). The EA corresponds to the energy difference between the N-electron and $N+1$-electron states, experimentally measured by gas-phase electron attachment spectroscopy. Note that E_{fund} relates to the energetic properties of a charged molecular species (anions and cations) rather than those of neutral molecules, as is the case of $E_{\text{HOMO–LUMO}}$ and the optical gap. The optical gap, E_{opt}, is the energy difference between the N-electron ground state (S_0) and the first (optically accessible) N-electron excited state (S_1) and is measured experimentally by gas-phase absorption spectroscopy. E_{opt} is smaller than E_{fund} due to the electrostatic interaction between the bound photoexcited electron–hole pair. The difference in energy $E_B = E_{\text{fund}} - E_{\text{opt}}$ is known has the electron–hole pair binding energy. Consequently, it can be generally stated that $E_{\text{HOMO}-\text{LUMO}} \neq E_{\text{fund}} \neq E_{\text{opt}}$.

2.2.2 Organic Solids

In the bulk of an organic solid, intermolecular interactions cause electronic delocalization and broadening of molecular levels into electronic bands with typically narrow bandwidths ca. <500 meV. The extent of electronic delocalization depends upon the strength of the electronic coupling between molecules as well as the energetic and positional disorder, both of which favor electronic localization. Organic solids display a wide range of molecular ordering depending on processing conditions and often combine in the same film highly crystalline, polycrystalline, or completely amorphous microscopic or nanoscopic domains [38]. The combined effects of electronic disorder at various length scales, electron–electron, electron–vibration interactions, and the low dielectric constant values displayed by organic materials (a consequence of the low atomic numbers of the atoms comprising organic molecules) result in poor Coulomb screening and high electronic localization [37].

Poor electrostatic screening and high electronic localization in organic materials cause electronic excitations and free charge carriers to display the following distinct characteristics.

Excitons. Electron–hole pairs bound under their Coulomb attraction are known as excitons. Excitons can be generated via photoexcitation or by association of a free electron and a free hole under their electrostatic attraction. Excitons are treated as neutral quasiparticles that diffuse via energy transfer processes involving either (a) radiative energy transfer (i.e., the emission and reabsorption of a photon) or (b) nonradiative energy transfer processes (Förster or Dexter energy transfer [39]).

Excitons play a prominent role in the molecular description of photogeneration and recombination processes in organic solids. Excitons in these materials, known as Frenkel excitons, are characterized by exciton binding energy values that are typically at least one order of magnitude larger than the thermal energy at room temperature, ca. 26 meV. In organic solids, Frenkel excitons are typically confined to single molecules or nearest neighboring molecules and display typical radius ca. 1 nm. In contrast, inorganic semiconductors display large dielectric constant values, high electrostatic screening, and exciton binding energy values smaller than the thermal energy. Consequently, even at room temperature, the thermal energy is sufficient to dissociate photogenerated excitons into free charge carriers. These types of excitons, known as Wannier excitons, are highly delocalized over several lattice constants, with typical radius ca. 10 nm.

Polarons. A free charge carrier in an organic solid induces ultrafast molecular vibrations that result in a strong polarization response of molecules and surrounding media, altering the electronic distribution and position of atoms and resulting in the formation of quasi particles known as polarons. The energy required for the geometrical reconfiguration of the molecule is known as the reorganization energy and represents the polaron binding energy. Polarons are quasi particles that describe a free charge carrier surrounded by a polarized media. Consequently, polarons display larger effective mass values than the ones associated with a free charge

carrier in its corresponding electronic band. The larger the effective mass of a polaron, the more localized its wave function. Highly localized polarons are referred to as small polarons and are typically found in organic solids. Polarons can move by tunneling, between equivalent localized polaron states, or by hopping between non-equivalent localized states, thus requiring the emission or absorption of a phonon. Tunneling results in band-like transport characteristics and is typically the dominant process at very low temperatures. Hopping is a thermally activated process mediated by electron–phonon interactions and is typically dominant at room temperature.

In an organic solid, a wide distribution of intermolecular interactions leads to homogeneous broadening of the distribution of energy states in a band (e.g. a bonding or antibonding band). Consequently, the minimum energy required to remove an electron, IE, and the energy gained by adding a negative charge carrier, EA, are different and smaller in the bulk than at the molecular scale. The energy difference $\mathrm{IE} - \mathrm{EA} \equiv E_{\mathrm{transport}}$ is known as the transport gap or bandgap, and in general, $E_{\mathrm{fund}} > E_{\mathrm{transport}}$. The IE of a solid is typically measured through UPS and the EA by inverse photoemission spectroscopy (IPES). Homogeneous broadening and the increased polarizability in the solid also leads to values of E_{opt} that are smaller than those found for isolated molecules in the gas or liquid phase. Nonetheless, since the exciton binding energy $E_{\mathrm{B}} = E_{\mathrm{transport}} - E_{\mathrm{opt}}$ (in the range from ca. 0.2 eV up to more than 1.0 eV) cannot be neglected, the absorption and emission processes take place at the single molecule or nearest neighbor molecular scale. Consequently, the oscillator strength associated with an electronic transition to a state that would be beyond the Coulomb capture radius, as required for an optical transition across $E_{\mathrm{transport}}$, is negligibly small. Finally, as in the molecular case, it should be clear that in general $E_{\mathrm{HOMO-LUMO}} \neq E_{\mathrm{transport}} \neq E_{\mathrm{opt}}$. Figure 2.1 presents a summary of relevant energy levels in organic molecules and solids.

2.3 Charge Transport and Photogeneration in Organic Semiconductors

Current understanding of organic molecules and intermolecular interactions leads to well-defined guidelines for achieving high photogeneration efficiency and mobility values, including high degree of crystallinity with close π–π intermolecular stacking; extended π–π overlap; increased molecular planarity and rigidity to reduce the formation of lattice defects and thermal fluctuations [35, 40–42]. However, at the mesoscopic scale, much work still needs to be done to fully grasp the impact that molecular packing and disorder at different length scales has over electronic transport.

Elements of the theory of band-transport will be described in this section as an introduction to the general phenomena of charge transport in semiconductors. Solid-state physics textbooks [43–46] offer detailed presentations of this material,

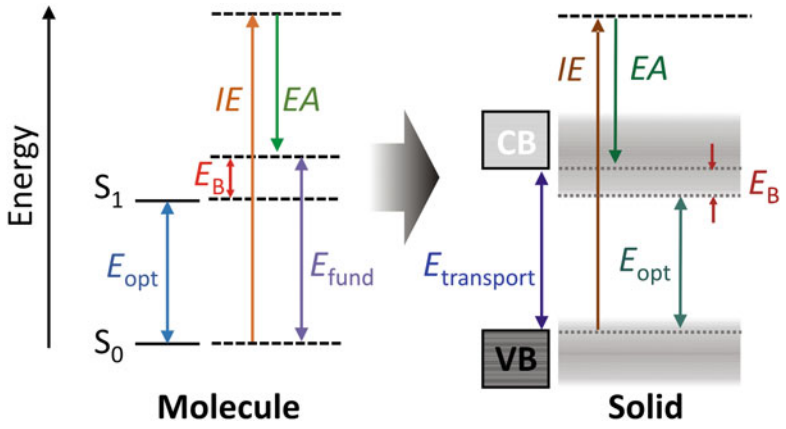

Fig. 2.1 Comparison of definition of energy gaps in organic molecules and solids

in particular for the case of crystalline semiconductors. However, organic photorefractive materials in general, and photorefractive polymers in particular, are typically classified as amorphous semiconductors [47, 48]. Charge transport and photogeneration of charge carriers in amorphous semiconductors cannot be described within the framework of band transport theory. Consequently, current theoretical descriptions of charge transport and photogeneration in amorphous semiconductors will also be reviewed in this chapter.

2.3.1 Semiconductors in Thermodynamic Equilibrium

2.3.1.1 Electronic Structure

Electrons in an atom display atomic orbitals represented by stationary electronic wave functions having quantized energy values. In a two-atom system, two valence-electron atomic orbitals, one from each atom, mix to form a chemical bond. A chemical bond results in two molecular orbitals: (1) a bonding orbital, where the electron density between the two nuclei of the atoms increases, resulting in a lower energy level than the energy level of the individual valence-electron atomic orbitals and (2) an antibonding orbital, where the electron density between the nuclei of the two atoms decreases, resulting in a higher energy level than the energy level of the individual valence-electron atomic orbitals. In a solid, a very large number of electrons interact, producing a large set of bonding orbitals with discrete energy values, and an analogous set of antibonding orbitals. These sets of bonding and antibonding orbitals having discrete but very closely spaced energy levels are referred to as energy bands, and are commonly approximated as a continuous set of energy levels.

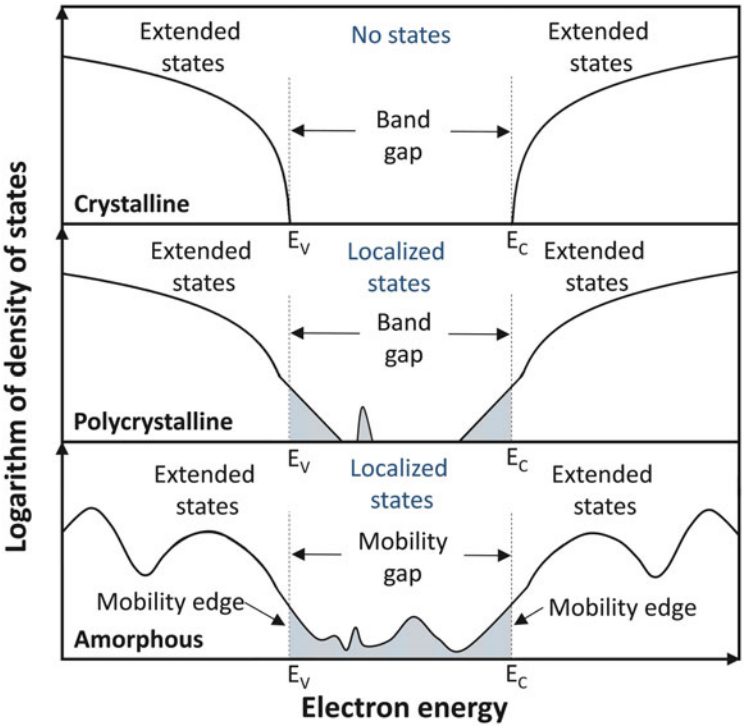

Fig. 2.2 Density of states distribution in crystalline, polycrystalline, and amorphous solids

In an ideal crystalline solid, atoms are periodically arranged with electronic wave functions that significantly overlap causing molecular orbitals to acquire long-range crystalline symmetries of the material. Disruption of these crystalline symmetries and the existence of long range order open up sharp energy gaps where no electronic states exist (see Fig. 2.2). The energy bands in crystalline materials display a well-defined relation with respect to the wave vector of an electron and give rise to what is commonly known as the band structure of the material, characterized by a function $E(\mathbf{k})$, where E is the energy and $\mathbf{k}$ the wave vector. In real crystalline solids, defects arising from disruption of the crystalline order are always present. Defects introduce localized energy states within the bandgap that can act as trapping sites or as electron-donating or electron-accepting states, leading to electronic doping of the solid. The electronic and optical properties of crystalline semiconductors are properly described by band theory. Band theory is a one-electron independent particle theory that intrinsically assumes the existence of a set of stationary extended one-electron states distributed according to Fermi-Dirac statistics.

In polycrystalline solids, atoms are arranged periodically but only within finite crystalline grains separated by grain boundaries. Grain boundaries and other defects

such as impurities or lattice dislocations introduce new electronic levels that are typically localized (i.e., the wave function has a negligible amplitude beyond a few nearest neighboring atoms) and with energies that lie within the bandgaps of crystalline phases of the material. Often times, a large density of grain boundaries results in a continuum of localized tail states that extends the energy bands into the bandgap (see Fig. 2.2).

In crystalline or polycrystalline organic solids, even in the presence of long-range order, the limited overlap of the molecular wave functions leads to energy bands with band widths (typically < 500 meV) narrower than those found in crystalline inorganic semiconductors.

Energy bands are nonetheless formed in solids even in the absence of the long-range order found in crystalline or polycrystalline materials. Even in the presence of strong disorder, amorphous solids still display short-range order and extended electronic states with narrow band widths. However, disorder-induced localized states, an intrinsic characteristic of amorphous solids, lead to a continuum of extended and localized electronic states with no appreciable bandgaps (see Fig. 2.2). Localization of electronic wave functions can arise when the random component of the potential disorder is larger than the band width (Anderson localization [49, 50]) or from electronic correlations (Mott-Hubbard transition [50]); a "many-body effect" induced by increased Coulomb repulsion as charge carriers become in close proximity. Localization and charge transport in amorphous solids cannot be described using band theory. Band theory predicts that increased localization of the wave function leads to an increased kinetic-energy contribution to the total energy and to energy bands with decreased bandwidth. Conversely, the increased delocalization of the electronic wave function leads to a reduction of the kinetic energy contribution to total energy and to energy bands with increased band width. However, in amorphous materials, when the potential disorder exceeds the band width, all states become localized around the Fermi level, and the material becomes an insulator known as a "Fermi glass"; a continuum of localized states occupied according to Fermi-Dirac statistics wherein states at the Fermi level are localized.

2.3.1.2 Electronic Occupation

Any description of charge transport in a solid relies on some knowledge of the distribution of energetic states within the relevant energy bands. This distribution, known as the density of states (DOS), $N(E)$, is obtained by counting the number of energetic states available for an electron with energy in the range between E and $E + \Delta E$ and can be defined as:

$$N(E) = \frac{1}{V} \frac{d\Omega(E)}{dE}, \tag{2.1}$$

where V is the volume and $\Omega(E)$ is the number of energy states.

The number of electrons occupying such energy states with an energy between E and $E + \Delta E$ can then be calculated as:

$$n(E,T)dE = N(E)f(E,T)dE, \tag{2.2}$$

where $f(E,T)$ is probability of finding an electron with a given energy E. Since electrons (and holes) are fermions, subatomic particles with spin ½, in thermodynamic equilibrium they display an energy distribution that follows Fermi-Dirac statistics, with a probability function given by the expression:

$$f(E,T) = \frac{1}{1 + \exp\left[{}^{(E-\varepsilon_F)}/_{kT}\right]}, \tag{2.3}$$

where ε_F is the chemical potential, $k = 1.38 \times 10^{-23}$ J/K $= 8.62 \times 10^{-5}$ eV/K is the Boltzmann constant, and T is the temperature. The chemical potential is derived, *in thermodynamic equilibrium*, as the rate of change in Gibbs free energy of a system, $G = U - pV - TS$ (where U is the internal energy, p is the pressure, V is the volume, and S the entropy) as a function of a change in the number of particles of a particular species (N). This is: $\varepsilon_F(T,V,N) \equiv (\partial G/\partial N)_{T,V}$. It is important to emphasize that $\varepsilon_F(T,V,N)$ has no meaning in non-equilibrium conditions.

In semiconductor physics, the chemical potential is commonly referred to as the Fermi level, $\varepsilon_F \equiv \varepsilon_F(T, V, N)$. This is an unfortunate selection of words inherited from derivations of the chemical potential in metals, where the Fermi level lies within the conduction band; however, in semiconductors or insulators, the Fermi level lies within the bandgap and does not correspond with a physical electronic level in the solid. Furthermore, the Fermi level must not be confused with the Fermi energy, E_F, defined as $\varepsilon_F(T = 0) \equiv E_F$ and consequently $\varepsilon_F(T) \neq E_F$. With this in mind, hereon we will refer interchangeably to $\varepsilon_F(T)$ as the chemical potential or Fermi level.

The relative position of the Fermi level with respect to the transport levels, conduction and valence bands, determines the electronic properties of the solid. In crystalline and polycrystalline materials, the conduction of electricity is exclusively related to electrons found in partially filled bands. In a metal, the Fermi level lies within one band which is partially filled even as T approaches absolute zero. In an insulator, all bands are completely filled or completely empty and the Fermi level lies within the transport bandgap of the material. In an insulator at room temperature there is a nonvanishing probability that some electrons will be thermally excited across the bandgap into the lowest unoccupied bands, the conduction bands. This thermal excitation leaves unoccupied electronic levels, holes, in the highest occupied bands, known as valence bands. Insulators where the thermal excitation across the bandgap leads to a significant density of charge carriers are referred to as semiconductors.

In amorphous materials no energy bandgap exists, but rather, a continuum of states forming energy bands of extended states and highly localized states at their tails. The transition between localized and extended states defines what is known as

the mobility edge. The separation that exists between the mobility edge in the conduction and the valence band in an amorphous material is known as the mobility gap, and plays an analogous role to the transport bandgap in a crystalline semiconductor. However, it should be stretched that the electronic properties in amorphous materials are not only a function of the position of the Fermi level with respect to the mobility edges, but also a function of the electronic localization (arising from disorder) around the Fermi level.

2.3.2 Intrinsic Semiconductors

A semiconductor in thermal equilibrium exhibits an intrinsic concentration of thermally generated charge carriers, $n_i(T)$, which is a function of the density of electrons in the conduction band and holes in the valence band ($n_c(T)$ and $p_v(T)$, respectively), and that can be calculated through the law of mass action as:

$$n_i(T) = [n_c(T)p_v(T)]^{1/2}. \tag{2.4}$$

Using Fermi-Dirac statistics and neglecting impurity levels, the density of electrons and holes follow an Arrhenius-like functional dependence of the form:

$$\begin{aligned} n_c(T) &= N_c(T)\exp\left(-\frac{E_c - \varepsilon_F}{kT}\right), \\ p_v(T) &= N_v(T)\exp\left(-\frac{\varepsilon_F - E_v}{kT}\right), \\ n_i(T) &= [N_c(T)N_v(T)]^{1/2}\exp\left(\frac{-\frac{1}{2}E_g}{kT}\right), \end{aligned} \tag{2.5}$$

where $N_{c,v}(T)$ are the DOS in the conduction and valence bands, respectively; and $E_g = E_c - E_v = E_{transport}$.

Even though in real semiconductors impurities cannot be avoided, a sufficient condition to define an intrinsic semiconductor can be written as:

$$\begin{aligned} E_c - \varepsilon_{F,i}(T) &\gg kT, \\ \varepsilon_{F,i}(T) - E_v &\gg kT. \end{aligned} \tag{2.6}$$

From this expression, the Fermi level of an intrinsic semiconductor can be calculated as:

$$\varepsilon_{F,i}(T) = E_v + \frac{1}{2}E_g + \frac{1}{2}kT\ln\left(\frac{N_v(T)}{N_c(T)}\right). \tag{2.7}$$

Note that since $\ln(N_v(T)/N_c(T))$ is of order one, this equation implies that when $kT < E_g$, the Fermi level lies far from either E_c or E_v, more specifically, in the middle of the bandgap: $\varepsilon_{F,i}(T \to 0) = E_v + \frac{1}{2}E_g$.

2.3.3 Extrinsic Semiconductors

Extrinsic semiconductors are materials where impurities produce significant amounts of free carriers. Impurities introduce electron orbital levels that are characterized as electron donor impurities, with a density N_D, or electron accepting impurities, with a density N_A. Donor impurities of energy ε_d are typically empty, or contain one electron of either spin. Acceptor impurities of energy ε_a are either singly occupied or, rarely, doubly occupied but not empty. If we consider the situation where the donor and acceptor levels are close to the edges of the gap:

$$\begin{aligned} \varepsilon_d - \varepsilon_F(T) &\ll kT, \\ \varepsilon_F(T) - \varepsilon_a &\ll kT, \end{aligned} \tag{2.8}$$

thermal excitation will fully ionize most impurities leading to: $N_d - N_a = n_c - p_v = \Delta n \neq 0$. Following the law of mass action, Eq. (2.4), allows expressing the carrier densities of extrinsic semiconductors in terms of their intrinsic carrier density values:

$$\begin{aligned} n_c &= \frac{1}{2}\left[(\Delta n)^2 + 4n_i^2\right]^{1/2} + \tfrac{1}{2}\Delta n, \\ p_v &= \frac{1}{2}\left[(\Delta n)^2 + 4n_i^2\right]^{1/2} - \tfrac{1}{2}\Delta n. \end{aligned} \tag{2.9}$$

If $\Delta n \geq n_i$, then the density of one carrier type approaches the value Δn, while the other is reduced by the differential factor $(n_i/\Delta n)^2$. Therefore, if impurities are the primary source of charge carriers in the bulk, the difference $N_d - N_a$ will then determine if electron or holes are dominant. If electron donating impurities are dominant ($N_d > N_a$) the semiconductor is referred to as n-type, and if electron accepting impurities are dominant ($N_a > N_d$), as p-type. Using Eq. (2.8), it can also be shown that the Fermi level in an extrinsic semiconductor is given by:

$$\frac{\Delta n}{n_i} = 2\sinh\left(\frac{\varepsilon_F - \varepsilon_{F,i}}{kT}\right). \tag{2.10}$$

2.3.3.1 Doping of Organic Semiconductors

Organic semiconductors are generally considered to be intrinsic semiconductors because no dopants are intentionally introduced. However, it is now well

recognized that gas molecules such as molecular oxygen, can lead to unintentional doping [51, 52]. Although intentional doping of organic semiconductors was reported since the early days [53], in recent years increased attention has been devoted to identification and development of dopant molecules having strong oxidizing (*p*-type dopants) or reducing (*n*-type dopants) potentials [51, 54–56]. Molecular dopants in organic semiconductors are introduced as interstitials instead of being covalently bound, as is typically the case in inorganic semiconductors. The interstitial nature of dopant molecules in organic semiconductors presents a challenge because they can diffuse into unwanted regions of a device and, in large concentrations, contribute significantly to the disorder in the solid [56–58]. However, in solids having initially low charge carrier densities and where the presence of disorder leads to the formation of localized states that can act as charge traps, even at low levels, doping can result in a dramatic increase of the conductivity that arises not only from an increased charge carrier density, as would be expected, but also from an increased charge mobility, since trap-filling leads to a reduced activation energy of the charge hopping process [59].

In amorphous solids, the charge carrier concentration can indeed play an important role in affecting charge mobility in particular, and charge transport in general, making controlled doping a highly desirable approach to improve transport in the bulk [51, 53, 56, 59–62]. Furthermore, doping of contacts has already been shown to play an important role in optimizing charge injection or extraction in optoelectronic devices, and consequently in optimizing device performance [53, 60, 63–67].

2.3.4 Semiconductors in Non-equilibrium: Charge Transport Models

The creation or extraction of free charge carriers in a semiconductor disturbs the thermodynamic equilibrium and generates a dynamic response. This dynamic response is inherently a non-equilibrium phenomenon which involves the transport of charge carriers under the action of external forces such as electric, electromagnetic fields, temperature gradients, and chemical potentials. In this section we will concentrate on electronic transport arising from spatial variations of the electrochemical potential and assume the absence of thermal gradients.

At a fundamental level, electronic transport is a many body quantum mechanical problem which is computationally intractable over the typical dimensions of optoelectronic devices. Instead, transport models rely on approximations that aim at capturing the fundamental physical characteristics of electronic transport at the relevant scales. Quantum mechanical approaches can be used to describe transport in nanoscopic volumes containing small numbers of carriers where electronic correlations in space and time are considered as well as non-local effects. On larger length scales, mean-field approximations are used to reduce the *N*-body problem to an effective one-electron problem. If electrons are treated as classical particles,

electronic correlations and non-local effects arising from wave function interference are lost. The Boltzmann transport model (accounting for nonlocal transport effects arising from rapidly changing electric fields) and the drift-diffusion model are examples of the most commonly used semiclassical transport models [46]. In modern optoelectronic devices, and organic-based ones in particular, electronic transport is especially complex since multiple length-scale phenomena coexist, requiring multiple descriptions at different levels to capture the rich physical nature displayed by these devices. In the following section, we will describe some of the basic concepts governing the physics of semiconductors in non-equilibrium and its use in the derivation of the commonly used drift-diffusion model.

2.3.4.1 Quasi-Fermi Levels

Excess free charge carriers in a semiconductor, initially in thermal equilibrium, will rapidly exchange energy through electron–electron and electron-lattice scattering processes leading to the formation of thermal distributions of electrons in the conduction band and holes in the valence band. The emergence of these thermal distributions is referred to as thermalization and typically occurs in subpicosecond time scales. These thermal distributions are in quasi-static equilibrium and follow Fermi-Dirac statistics, but do not share the same Fermi level since they are not in thermodynamic equilibrium with each other. The Fermi levels associated with these distributions are consequently called the "quasi-Fermi levels," $\varepsilon_{\mathrm{f}n}$ and $\varepsilon_{\mathrm{f}p}$, defined as:

$$\begin{aligned} n_{\mathrm{c}}(\mathbf{r},T) &= N_{\mathrm{c}}(T)\exp\left(-\frac{E_{\mathrm{c}}(\mathbf{r})-\varepsilon_{\mathrm{f}n}(\mathbf{r})}{kT}\right), \\ p_{\mathrm{v}}(\mathbf{r},T) &= N_{\mathrm{v}}(T)\exp\left(-\frac{\varepsilon_{\mathrm{f}p}(\mathbf{r})-E_{\mathrm{v}}(\mathbf{r})}{kT}\right). \end{aligned} \tag{2.11}$$

Under these conditions, the law of mass action is no longer valid in its original form, since carriers have been added ($n_{\mathrm{c}}p_{\mathrm{v}} > n_i^2$) or removed ($n_{\mathrm{c}}p_{\mathrm{v}} < n_i^2$), but can be modified into the following expression:

$$n_{\mathrm{c}}(T)p_{\mathrm{v}}(T) = [n_i(T)]^2 \exp\left(\frac{\varepsilon_{\mathrm{f}n}-\varepsilon_{\mathrm{f}p}}{kT}\right). \tag{2.12}$$

Hence, $\left|\varepsilon_{\mathrm{f}n}-\varepsilon_{\mathrm{f}p}\right|$ represents a measure of how far from equilibrium is the semiconductor.

2.3.4.2 Drift-Diffusion Model

The drift-diffusion model is probably the most commonly used approach to describe charge transport in semiconductors. The model is built on two basic assumptions:

1. Charge carriers are classical particles that obey Newton's laws.
2. Charge carriers are in local equilibrium, undergoing several collisions before the forces driving them change significantly in space or time.

As the name of the model implies, electric currents are assumed to be the result of two processes: *drifting* under an applied electric field and *diffusing* from regions of high carrier concentration to regions of lower carrier concentration. Although these two contributions are commonly defined separately for historic reasons, it is worth stressing the fact that they arise from the non-equilibrium considerations that led us to define the quasi-Fermi levels through Eq. (2.11). Remembering that the quasi-Fermi level is also the electrochemical potential, the force field associated with this potential energy, what could be called the electrochemical force, can be calculated as:

$$\begin{aligned} \nabla \varepsilon_{\mathrm{fn}}(\mathbf{r},T) &= \nabla E_{\mathrm{c}}(\mathbf{r}) + kT\frac{\nabla n_{\mathrm{c}}(\mathbf{r},T)}{n_{\mathrm{c}}(\mathbf{r},T)}, \\ \nabla \varepsilon_{\mathrm{fp}}(\mathbf{r},T) &= \nabla E_{\mathrm{v}}(\mathbf{r}) - kT\frac{\nabla p_{\mathrm{v}}(\mathbf{r},T)}{p_{\mathrm{v}}(\mathbf{r},T)}. \end{aligned} \tag{2.13}$$

The first terms on the right-hand side of Eq. (2.13) can be identified as an electric force: $q\mathbf{F} = \nabla E_{\mathrm{c,v}}(\mathbf{r})$, where $\mathbf{F}$ is the local electric field and $q = 1.9 \times 10^{-19}$ C is the elementary charge. The second term on the right-hand side of Eq. (2.13) is a force driven by a concentration gradient, a diffusion force.

The current density is proportional to the total force per unit charge, and can be expressed as:

$$\begin{aligned} \mathbf{j} &= \sum_{i=n,p} \sigma_i(T)\frac{\nabla \varepsilon_{\mathrm{f}i}(\mathbf{r},T)}{q} \\ &= \mathbf{j}_{\mathrm{drift}} + \mathbf{j}_{\mathrm{diffusion}}. \end{aligned} \tag{2.14}$$

The constant of proportionality, $\sigma(T)$, known as the conductivity, is material dependent and may not be a scalar but a tensor. From Eq. (2.13), we conclude that the emergence of the quasi-Fermi energy in a semiconductor in non-equilibrium, leads to the flow of two types of electrical currents: drift and diffusion. The drift current is associated with the terms:

$$\mathbf{j}_{\mathrm{drift}} = \left[\sigma_n(T) + \sigma_p(T)\right]\mathbf{F} \tag{2.15}$$

known as Ohm's law. The diffusion current is associated with the terms:

$$\mathbf{j}_{\mathrm{diffusion}} = \frac{kT}{q}\left[\frac{\sigma_n(T)}{n_{\mathrm{c}}(\mathbf{r},T)}\nabla n_{\mathrm{c}}(\mathbf{r},T) - \frac{\sigma_p(T)}{p_{\mathrm{v}}(\mathbf{r},T)}\nabla p_{\mathrm{v}}(\mathbf{r},T)\right]. \tag{2.16}$$

2.3.4.3 Conductivity

The conductivity can be generally classified as: intrinsic, if carriers are generated thermally; extrinsic, if carriers are generated by impurities or dopants; injection-controlled, if carriers are injected into the material through a conducting electrode; and photoconductivity, if carriers are generated through the absorption of light. From this classification, it should be clear that in general, the conductivity of a solid can originate from several physical processes acting in parallel.

The conductivity can be derived using Newton's second law by assuming that magnetic interactions can be neglected and that the forces acting on an electron are the electrochemical force and a scattering force acting in the opposite direction. If the scattering force is taken as a frictional force of the form: $-m_n^*\mathbf{u}_n/\tau_n$ (known as Drude's assumption) where τ_n is the average time between collisions, m_n^* is the electron's effective mass, and $\mathbf{u}_n$ is the average velocity of electrons, then, under steady-state conditions:

$$-\frac{m_n^*\mathbf{u}_n(\mathbf{r})}{\tau_n(T)} = q\frac{\nabla\varepsilon_{\mathrm{f}n}(\mathbf{r},T)}{q}. \tag{2.17}$$

Note that since by definition, $\mathbf{j}_n = -qn_{\mathrm{c}}(T)\mathbf{u}_n(T)$, we can derive the following expressions:

$$\begin{aligned}\sigma_n &= q^2 n_{\mathrm{c}}(T)\frac{\tau_n(T)}{m_n^*} = qn_{\mathrm{c}}(T)\mu_n(T),\\ \mu_n(T) &\equiv q\frac{\tau_n(T)}{m_n^*}.\end{aligned} \tag{2.18}$$

Analogous expressions can also be derived for the conductivity of holes.

The average collision time is a temperature-dependent quantity because electronic scattering processes in a solid, such as scattering with phonons (quantized vibrational lattice modes), scattering with ionized defects, such as trapped charges, are temperature-dependent processes. The parameter $\mu_{n,p}(T)$ is known as the electron or hole drift mobility and represents the average drift velocity per unit electric field. Inserting Eq. (2.18) into Eq. (2.16) allows expressing the diffusion current in the more familiar form of Fick's law of diffusion:

$$\mathbf{j}_{\mathrm{diff}} = q\big(D_n\nabla n_{\mathrm{c}} - D_p\nabla p_{\mathrm{c}}\big), \tag{2.19}$$

where D_n and D_p are the electron and hole diffusion coefficients, respectively, and where we have also assumed that the Einstein relation: $\mu_{n,p}(T)kT = qD_{n,p}(T)$ is valid. In disordered organic semiconductors, the Einstein relation has been shown to be violated under nonequilibrium conditions in the presence of deep traps, and questioned even in the case of thermal equilibrium. However, recently it has been shown to be valid in thermal quasi-equilibrium and at low carrier concentrations and low electric fields [68, 69].

2.3.4.4 Equations of State

In addition to the drift and diffusion equations, a steady-state description of charge transport in a solid requires solving a set of five differential equations given by:

$$\begin{aligned} &\text{(Poisson equation)} && \nabla[\varepsilon(\mathbf{r})\mathbf{F}(\mathbf{r})] = q[p(\mathbf{r}) - n(\mathbf{r})] \\ &\text{(Continuity equations)} && \nabla\mathbf{J}_{n,p} + qG_{n,p}(\mathbf{r}) \mp qR_{n,p}(\mathbf{r}) = 0\,, \\ &\text{(Current equations)} && \mathbf{J}_{\text{drift},n,p} \pm \mathbf{J}_{\text{diffusion},n,p} = \mathbf{J}_{n,p} \end{aligned} \tag{2.20}$$

where $G_{n,p}(\mathbf{r})$ and $R_{n,p}(\mathbf{r})$ are the electron and hole generation and recombination rates. Relevant models to describe the physical parameters invoked in these equations will be discussed in the following sections.

2.3.5 Charge Transport in Organic Semiconductors

2.3.5.1 Electronic Coupling

At room temperature, most solids of interest display transport characteristics in the hopping regime wherein hopping events are described by incoherent electron-transfer reactions. Electron-transfer reactions are strongly dependent on electronic coupling. A detailed review of this subject is given in [42]. Electronic coupling between two charge-localized states $|\psi_a\rangle$ and $|\psi_b\rangle$ is given through the matrix element $t_{ab} = \langle\psi_a|H|\psi_b\rangle$ where H is the electronic Hamiltonian of the system.

In the absence of disorder, electronic states of a periodic array of molecules are expected to be given by Bloch states, constructed from the molecular orbitals of isolated molecules, and transport may be well approximated using band theory; this is $\mu(T) = q\tau(T)/m^*$, decreasing with increasing temperature.

In the presence of disorder, direct calculations of these transfer integrals are very challenging and often rely on major simplifications. The most frequently used simplification arises from combining the energy-splitting-in-dimer method and Koopmans theorem [42], and assumes a one-electron approximation leading to the magnitude of the transfer integral for an electron (hole) transfer from molecule M_a to M_b, expressed as:

$$t = \frac{E_{L+1[H]} - E_{L[H-1]}}{2}, \tag{2.21}$$

where $E_{L[H]}$ and $E_{L+1[H-1]}$ are the energies of the LUMO [HOMO] and LUMO + 1 [HOMO − 1] levels in a closed-shell configuration of the neutral state of the dimer $M_a - M_b$ calculated in the intermolecular packing configuration encountered in the bulk of the material.

2.3.5.2 Electron–Phonon Coupling

Free charge carriers in organic semiconductors are characterized as polarons. Polarons are classified as large or small depending on the size of the lattice distortion induced by a free charge carrier with respect to the lattice size. In molecular crystals, including organic materials, polarons are generally classified as small polarons. This is because the electron–phonon coupling is strong but of short range. For a polaron having a binding energy E_{pol}, the strength of the electron–phonon coupling is characterized by a coupling constant, g. If we assume that strong electron–phonon coupling leads to full localization of the charge, and consequently to a negligible transfer integral, the coupling constant between the polaron and an optical phonon of frequency ω_0 is given by $g = \sqrt{E_{\text{pol}}/\hbar\omega_0}$; if $g^2 \ll 1$ coupling is considered weak. If $g^2 \gg 1$ coupling is considered strong.

2.3.5.3 Polaron Model: The Holstein Model

Polarons can move through a succession of individual tunneling or hopping events between energetically available sites [42]. Most detailed polaron transport models are based on seminal work conducted by Holsetein [70, 71]. According to the Holstein polaron model, in solids with weak electron–phonon coupling ($g^2 \ll 1$), electrons are characterized as large polarons and charge transport is dominated by tunneling, leading to mobility values that display a band-like temperature dependence, i.e., $\mu \propto T^{-n}$ with $n > 0$. In solids with strong local electron–phonon coupling ($g^2 \gg 1$), electrons are characterized as small polarons and three different transport regimes are commonly found as a function of the solids temperature:

1. *Tunneling regime*. Electron tunneling arises from coherent electron transfer processes leading to mobility values that display band-like temperature dependence. At low temperatures, tunneling dominates the charge transport characteristics.
2. *Hopping regime*. As the temperature increases electron transfer becomes increasingly incoherent, until above a certain temperature T_1, charge transport in the solid is dominated by hopping. Hopping involves incoherent electron-transfer reactions between nearest-neighbors which are field-assisted and thermally activated through a manifold of states associated with neutral molecules. In the absence of direct carrier injection from the electrodes, hopping processes usually lead to unipolar transport. A thermally activated dependence of the mobility: $\mu \propto \exp(-\Delta/kT)$, leads to increasing mobility values with increasing temperature.
3. *Electron-scattering regime*. Finally if the temperature can be increased to high enough values to dissociate the polaron at a temperature T_2, the residual electron is scattered by thermal phonons and the mobility decreases again with increased temperature.

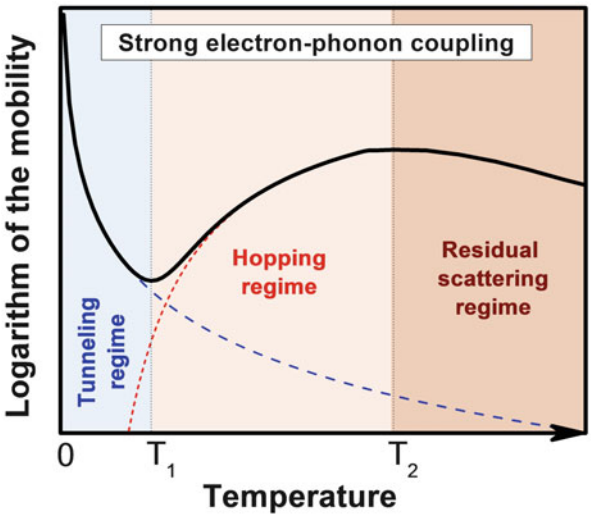

Fig. 2.3 The *black solid line* represents the temperature dependence of the mobility in the presence of strong electron–phonon coupling displaying the three characteristic transport regimes predicted by Holstein model. *Blue dashed line* represents $\mu \propto T^{-n}$ dependence. *Red dashed line* represents $\mu \propto \exp(-\Delta E/kT)$ dependence

Figure 2.3 displays the thermal dependence of the mobility for a small polaron solid as described by Holstein model. Note that according to this model, thermal dependent studies of the mobility could potentially be used to gauge the nature of charge transport in an organic solid.

In the hopping regime, the Holstein model [70, 71] of polaron transport uses perturbation theory to calculate the polaron hopping rate in the absence of chemical and physical defects or disorder, as:

$$\kappa_{\mathrm{ET}} = \frac{t^2}{\hbar^2\omega_0}\sqrt{\frac{\pi}{g^2\mathrm{csch}\left(\frac{\hbar\omega_0}{2kT}\right)}} \times \exp\left[-2g^2\tanh\left(\frac{\hbar\omega_0}{4kT}\right)\right]. \tag{2.22}$$

For a 1D system, the diffusion coefficient is given by $D = a^2\kappa_{\mathrm{ET}}$, where a denotes the spacing between molecules. Using Einstein's relation, the mobility in the hopping regime can be expressed as:

$$\mu_{\mathrm{hop}} = \frac{q}{kT}\frac{a^2t^2}{\hbar^2\omega_0}\sqrt{\frac{\pi}{g^2\mathrm{csch}\left(\frac{\hbar\omega_0}{2kT}\right)}} \times \exp\left[-2g^2\tanh\left(\frac{\hbar\omega_0}{4kT}\right)\right]. \tag{2.23}$$

In the classical limit, $\hbar\omega_0 \ll kT$, Eqs. (2.22) and (2.23) follow an Arrhenius temperature dependence with an activation energy $\frac{1}{2}E_{\mathrm{pol}}$. Note that $2E_{\mathrm{pol}} = \lambda_{\mathrm{reorg}}$, where λ_{reorg} is the so-called reorganization energy which equals the sum of the geometrical relaxation energies upon charging or discharging molecules during an intermolecular reaction of the type: $M_a^- - M_b \rightarrow M_a - M_b^-$. Expressing Eq. (2.22) as a function of λ_{reorg} allows recovering the familiar semiclassical expression

derived by Marcus [72]. As pointed by Holstein, perturbation theory cannot be applied for transfer integrals exceeding a critical value, requiring electron transfer processes to be treated adiabatically.

2.3.5.4 Disorder Models

The Holstein model explicitly excludes the presence of disorder in the solid. The presence of chemical or physical disorder leads to increasing localization of band states starting at the tail of the band and continuing until all states become localized in the case of strong disorder, such as in amorphous polymers. Since the transfer integral is very sensitive to intermolecular position and orientation it should be noted that thermal fluctuations (on a picosecond time scale) become an important source of dynamic disorder at room temperature, where the standard deviation of these fluctuations becomes of comparable order to the magnitude of the average transfer integral. In this regard, two main models have been used to calculate the hopping rate in the presence of static disorder and where electron-transfer reactions occur between nonequivalent hopping sites with energy values ε_i and ε_j. In both models, the hopping sites are assumed to be distributed following a Gaussian distribution DOS with standard deviation σ_{DOS}, from which potential hopping sites are randomly selected:

$$N_{\mathrm{c,v}}(E) = \frac{N_{\mathrm{t}}}{\sqrt{2\pi}\sigma_{\mathrm{DOS}}} \exp\left(-\frac{E^2}{2{\sigma_{\mathrm{DOS}}}^2}\right) \equiv g(E), \tag{2.24}$$

where N_{t} is the total DOS. Hereon the notation $g(E)$ will be used instead of $N_{\mathrm{c,v}}(E)$ to denote a Gaussian DOS [73].

2.3.6 Hopping Rate: Miller-Abrahams Model

The first hopping model originally developed by Miller-Abrahams [74] considers that the hopping rate κ_{ij} is given by the form:

$$\kappa_{ij} = \nu \exp\left(-2\gamma \Delta R_{ij}\right) \begin{cases} \exp\left[-\left(\dfrac{\varepsilon_j - \varepsilon_i}{kT}\right)\right] & \text{for } \varepsilon_j > \varepsilon_i \\ 1 & \text{for } \varepsilon_j < \varepsilon_i \end{cases}, \tag{2.25}$$

where ν is a prefactor related to the attempt hopping frequency, γ is the inverse wave function decay constant, and $\left|\Delta R_{ij}\right| = \left|R_i - R_j\right|$ the intersite distance. The Miller-Abrahams form was originally developed to describe charge hopping in crystalline materials with high trap densities [74]. In crystals, charge transport typically occurs through highly delocalized modes in the conduction band but the presence of high concentrations of trapping sites leads to multiple charge trapping

and detrapping events that closely resemble a charge hopping mechanism. It is worth pointing out, that implicit in the Miller-Abrahams form, it's assumed that charge hopping from high to low energy sites is not restricted by any condition for dissipating the energy difference between them, and that such downward jumps are not affected by the presence of an electric field. Therefore, effects arising from strong charge-phonon coupling are neglected.

2.3.7 Hopping Rate: Marcus Model

A more successful model to describe hopping in organic semiconductors is given by the expression for semiclassical electron-transfer rates provided by Marcus:

$$k_{ij} = \frac{t^2}{\hbar}\sqrt{\frac{\pi}{kT\lambda_{\text{reorg}}}}\exp\left(-2\gamma\Delta R_{ij}\right)\exp\left(-\frac{\left(\lambda_{\text{reorg}}+\varepsilon_j-\varepsilon_i\right)^2}{4\lambda_{\text{reorg}}kT}\right). \tag{2.26}$$

Unlike Miller-Abrahams theory, which leads to a monotonic increase in the hopping probability with increasing free-energy $\left|\Delta G^0\right| = \left|\varepsilon_j - \varepsilon_i\right|$, Marcus theory leads to two distinct regimes: (1) the normal regime, where $\lambda_{\text{reorg}} > \left|\Delta G^0\right|$ and the hopping rate increases with increasing value of $|\Delta G^0|$, until it reaches a maximum value when $\lambda_{\text{reorg}} = \left|\Delta G^0\right|$; after which (2) in the inverted regime, where $\lambda_{\text{reorg}} < \left|\Delta G^0\right|$, the hopping rate decreases with increasing value of $|\Delta G^0|$.

2.3.8 Poole-Frenkel Models

Early descriptions of hopping transport under an electric field in amorphous materials where done by Frenkel [75] on the basis of a field-induced reduction of the Coulomb potential barrier and in the context of photogeneration. Empirical equations for the mobility with a Poole-Frenkel dependence have the general form [76]:

$$\mu \propto \exp\left\{-\frac{\Delta_0 - \beta\sqrt{F}}{kT_{\text{m}}}\right\}, \tag{2.27}$$

where Δ_0 is the activation energy, β and T_{m} are constants experimentally determined. However, Poole-Frenkel models are based on a physically unrealistic assumption that requires Coulomb traps at each hopping site.

2.3.9 Gaussian Disorder Model

Over the years, a large variety of models have been developed to describe transport in amorphous semiconductors materials [42, 73, 77]. As demonstrated by Bässler and coworkers [78–81] Monte Carlo simulations have proven the simplest approach to describe transport in amorphous materials under an applied electric field. The empirical relations derived by Bässler and coworkers from their numerical results have gained acceptance since they have shown to be in agreement with experimental results obtained in a variety of amorphous organic materials such as polymer composites, main chain and pendant group polymers, and molecular glasses. The so-called disorder formalism assumes that the loss of long-range order creates a manifold of localized states with superimposed energetic and positional disorder within a Gaussian DOS. Positional disorder is assumed to result from local variations of the electronic coupling between nearest-neighbor hopping sites randomly distributed over space, described with the parameter Σ. The hopping rates are described by using the Miller-Abrahams model and the model assumes that coherence is lost after consecutive hopping events. Therefore, each hopping event can be treated as statistically independent. Using these assumptions over the hopping process, the mobility is given by:

$$\mu(\hat{\sigma}_{\mathrm{DOS}}, F) = \mu_0 \exp\left[-\left(\frac{2}{3}\hat{\sigma}_{\mathrm{DOS}}\right)^2\right] \exp\left\{C\left[(\hat{\sigma}_{\mathrm{DOS}})^2 - \Sigma^2\right]\sqrt{F}\right\} \quad \text{for } \Sigma \geq 1.5,$$

$$\mu(\hat{\sigma}_{\mathrm{DOS}}, F) = \mu_0 \exp\left[-\left(\frac{2}{3}\hat{\sigma}_{\mathrm{DOS}}\right)^2\right] \exp\left\{C\left[(\hat{\sigma}_{\mathrm{DOS}})^2 - 2.25\right]\sqrt{F}\right\} \text{ for } \Sigma \leq 1.5, \tag{2.28}$$

where μ_0 is a mobility prefactor, C an empirical constant with a value of 2.9×10^{-4} $(\mathrm{cm/V})^{1/2}$, and $\hat{\sigma}_{\mathrm{DOS}} = \sigma_{\mathrm{DOS}}/kT$. Note that Eq. (2.28) follows both an Arrhenius-like thermal dependence with activation energy equal to $\frac{2}{3}\sigma_{\mathrm{DOS}}$ and a Poole-Frenkel electric-field dependence.

2.3.9.1 Influence of Randomly Oriented Dipoles

The disorder formalism has been used to describe the electric field and temperature dependence of the mobility in photorefractive polymer composites [82] and the role of randomly oriented dipoles (provided by the presence of chromophores) described on the basis of two statistical independent contributions [83–85]: the usual Van der Waals contribution $\widetilde{\sigma}_{\mathrm{VdW}}$ and a dipolar contribution $\widetilde{\sigma}_{\mathrm{d}}$ with a general form:

$$\widetilde{\sigma}_{\mathrm{d}} = k_0 \frac{c^n}{\varepsilon a^m} \left|\vec{p}\right|, \tag{2.29}$$

where $\vec{p}$ is the dipole moment of the dopant molecules, ϵ the dielectric constant, c is the concentration of dipoles, a is the average intersite distance, and k_0, n, and m are constants which values differ within the models [83–86]. Given the statistical independence of the contributions, the total width of the energetic disorder is then calculated as:

$$\sigma_{\mathrm{DOS}}^2 = \widetilde{\sigma}_{\mathrm{VdW}}^2 + \widetilde{\sigma}_{\mathrm{d}}^2. \tag{2.30}$$

There's also experimental evidence [82, 87] showing that the dipolar disorder also affects the off-diagonal disorder parameter Σ. However, no model has yet been produced to describe the observed effects produced by the presence of highly polar molecules and to provide a consistent physical description of such polymer composites.

2.4 Correlated Gaussian Disorder Model (CGDM): Energy Site Correlations

The disorder formalism provides good agreement with experimental data provided μ_0, σ_{DOS}, and Σ are regarded as fitting parameters. However, for molecularly doped polymers, values of σ_{DOS} derived through the model do not yield realistic estimations of the widths of the DOS. A further refinement of the model was carried out through extensive simulations of a 3D disorder model that considered spatial correlations due to charge-dipole interactions [86, 88]. Such simulations produced the following expression for non-dispersive transport:

$$\mu(F,T) = \mu_0 \exp\left[-\left(\frac{3}{5}\frac{\sigma_{\mathrm{DOS}}}{kT}\right)^2\right] \exp\left\{C_0\left[\left(\frac{\sigma_{\mathrm{DOS}}}{kT}\right)^{3/2} - \Gamma\right]\sqrt{\frac{qaF}{\sigma_{\mathrm{DOS}}}}\right\}, \tag{2.31}$$

where a is the minimal charge-dipole separation and can be regarded as the size of a cubic lattice with randomly oriented dipoles at each vertex; Γ characterizes the geometric disorder and can be regarded as analogous to Σ^2, C_0 has a value of 0.78, and q is the elementary charge. Such form is supported by the development of an analytic effective-medium theory [89] which used a modified expression for the jump rates to describe charge transport in weakly disordered materials within the framework of the disorder formalism, and later expanded its approach to describe non-dispersive transport in materials containing traps [90, 91].

2.5 Effective Medium Model: Polaron and Disorder Effects

It should be noted that Holstein model of polaron transport disregards the effects of energetic disorder, specifically as a contribution to the activation energy of charge mobility. On the other hand, all models herein described based on the Gaussian disorder model disregard polaronic effects so that the activation energy of the charge transport reflects only the static energetic disorder of the hopping sites. Indeed, discrimination between both effects can be rather difficult [92, 93] as both relate to the energetic disorder experienced by a charge in the solid, albeit at presumably different time scales. In addition, Gaussian disorder models have been developed following Miller-Abrahams formalism instead of Marcus theory. An analytical theory based upon an effective medium approach that considers the superposition of disorder and polaron effects and that treats the hopping rates following Marcus theory as well as energy site correlations was developed by Fishchuk and coworkers [93]. Within this theory, the mobility is given by:

$$\mu(\hat{\sigma}_{\mathrm{DOS}}, F) = \mu_0 \exp\left[-\frac{E_a}{kT} - \frac{\hat{\sigma}_{\mathrm{DOS}}^{\,2}}{8\zeta}\right] \exp\left\{\frac{\hat{\sigma}_{\mathrm{DOS}}^{\,3/2}}{2\sqrt{2}\zeta}\sqrt{\frac{qaF}{\sigma_{\mathrm{DOS}}}}\left(1 - \frac{1}{\hat{\sigma}_{\mathrm{DOS}}}\right)\right\}, \quad (2.32)$$

$$\zeta = 1 - \frac{\sigma_{\mathrm{DOS}}^2}{8qakT}$$

where E_a is half the polaron binding energy.

2.6 Extended Gaussian Disorder Model: Carrier Concentration Dependence

Models described to this point are in principle not applicable to materials having a high concentration of free charge carriers, on the order of 10^{18}–10^{19} cm^{-3}. The dependence of the mobility on the charge carrier concentration has been extensively discussed in the context of organic field-effect transistors, where carrier densities can be varied by several orders of magnitude [94–97]. This dependence has been rationalized within the context of the extended Gaussian disorder model (EGDM) by assuming that the tail states in a Gaussian DOS will be more localized compared to states closer to the center, leading to two distinct transport regimes [77, 98]:

Regime 1: A low mobility regime at low carrier-densities where mobile carriers move by hopping through a manifold of localized states at the tail of the Gaussian DOS distribution. In this regime, carriers can be trapped in states having an energy much larger than their thermal energy and the mobility is independent of the carrier concentration. Therefore, if $E_F \ll -\sigma_{\mathrm{DOS}}^2/kT \equiv E_0$, the shape of the energy distribution of occupied states (i.e. the product of the Gaussian DOS times the Fermi-Dirac distribution function) is approximately a Gaussian centered at E_0; the

so-called thermal equilibrium energy, which represents the averge carrier energy in this regime.

Regime 2: As the carrier concentration, $c(E) = n(E)/N_t$, passes certain threshold, the mobility increases since states at the tail of the DOS become filled and carriers are less likely to be trapped in deep trapping states. The threshold between these two regimes is expressed by the condition: $E_F = E_0$ and corresponds to a carrier concentration:

$$c(E_F = E_0) = \frac{1}{2}\exp\left(\frac{E_0}{2kT}\right). \tag{2.33}$$

Within this model, it can be shown that the mobility depends on the carrier concentration as:

$$\mu(c) = \mu_{0,\mathrm{EGDM}}\frac{1}{c}\exp\left(\frac{E_F(c)}{kT} - \frac{E_0}{2kT}\right), \tag{2.34}$$

where $\mu_{0,\mathrm{EGDM}}$ is the zero-field mobility; noting that $\mu(E_F = E_0) = 2\mu_{0,\mathrm{EGDM}}$. To get a sense of the concentrations involved in these limits let's consider that a typical $\sigma_{\mathrm{DOS}} = 0.1\,\mathrm{eV}$ [87] at room temperature will lead to $E_0 = -0.4\,\mathrm{eV}$ and to $c(E_F = E_0)$ca. 10^{-4} or $n(E_0) \approx 10^{-4}N_t$.

Using 3D Monte Carlo modeling, it was found that as the carrier concentration increases to values ca. 10^{-2}, repulsive Coulomb interactions become important, leading to decreased mobility values [99]. The results from this simulation were shown to be well described by the following 1D expression for the mobility [98]:

$$\begin{aligned}
\mu(\hat{\sigma}_{\mathrm{DOS}}, c, F) &= \mu_{0,\mathrm{EGDM}}(T)\exp\left[\frac{1}{2}\left(\hat{\sigma}^2_{\mathrm{DOS}} - \hat{\sigma}_{\mathrm{DOS}}\right)(2c)^{\delta}\right] \\
&\quad \times \exp\left[0.44\left(\hat{\sigma}^{3/2} - 2.2\right)\left(\sqrt{1 + 0.8\hat{F}^2} - 1\right)\right], \\
\sigma_{\mathrm{DOS}} &\equiv \frac{\sigma_{\mathrm{DOS}}}{kT}; \\
\hat{F} &\equiv \frac{qaF}{\sigma_{\mathrm{DOS}}}; \\
\delta &\equiv \frac{2}{\hat{\sigma}^2_{\mathrm{DOS}}}\left[\ln\left(\hat{\sigma}^2_{\mathrm{DOS}} - \hat{\sigma}_{\mathrm{DOS}}\right) - \ln(\ln 4)\right],
\end{aligned} \tag{2.35}$$

where a is the intermolecular distance. This parametrization has been shown to be accurate to values of c ca. 0.1 and up to electric fields ca. 200 V/μm [99]. The presence of dipole moments, quadrupolar moments, long-range thermal fluctuations, or short-range order due to molecular packing can also lead to spatially correlated energy levels within the DOS. Models, such as the extended correlated disorder model (ECDM), have been proposed to take into account such correlations. An extensive review of these and other relevant models to describe charge transport in disordered organic materials can be found in [77, 98, 100].

2.7 Guest–Host Material Systems

Finally, it should be pointed out that organic photorefractive polymers can display a level of complexity that goes beyond the material systems previously described. This is because photorefractive polymers typically comprise a polymer host that is heavily doped with several guest molecules providing the functionalities needed for the material to display photorefractive properties (i.e., highly polar electro-optic molecules, charge-transport moieties, sensitizers, and plasticizers). In guest–host systems, the energy landscape that carriers experience in the transport manifold, typically thought to be defined by the guest polymer, is severely affected by the presence of localized molecular states, induced by either positional or energetic disorder or by the intrinsic electronic structure of the guest molecules, acting as shallow or deep traps. The density and distribution of such localized states are indeed critical in defining the temporal response and operational stability of photorefractive polymers [30, 101–107].

In a very simplified picture, guest–host systems wherein the guest energy defines a DOS with a central energy, E_T, such as it acts as a trap with respect to the host transport manifold, displays four transport regimes depending on the guest concentration [97]:

1. At very low guest concentrations, transport is dominated by host-to-host hopping events, and guest molecules act as traps but do not have major impact on transport.
2. As the guest concentration increases, they start acting as trap sites. In this regime and for small electric fields, the mobility can be described by a multiple-trap-release thermal and field-induced detrapping model, and becomes dependent on the carrier density as described by the EGDM.
3. At intermediate guest concentrations, hopping takes place through both the host and guest manifolds. In this region of transition, no good model currently exists to describe the random statistical variations of local guest and host concentrations.
4. As the guest concentration increases, transport becomes dominated by guest-to-guest hopping events and the mobility increases rapidly as the distance between guest molecules decreases.

2.7.1 Photoconductivity in Organic Materials

The generation of free charge carriers through the absorption of light constitutes one of the most important physical phenomena in solid-state materials. A photon of light is absorbed in a material when the energy of the photon, $h\nu$, matches the energy difference between an occupied and an empty (optically allowed) electronic state. As discussed, in inorganic materials, the minimum energy at which this electronic transition occurs is, to a good approximation,

$E_{opt} \equiv h\nu_{min} \approx E_g$, while in an organic material, the minimum energy is equal to $E_{opt} = E_{transport} - E_B$.

Beyond this simple picture, we should note that the absorption of light in a solid can arise from a wide variety of physical phenomena. For instance, photon–phonon interactions can lead to phonon assisted absorption as in the case of indirect gap semiconductors. Nonlinear optical processes can also lead to the absorption of light at sufficiently high irradiance values through the absorption of multiple photons having energies well below the optical bandgap of the material but fulfilling the condition:

$$\sum_{i>1} h\nu_i \geq E_{opt}. \tag{2.36}$$

For instance, in the case of a two-photon absorption (TPA) process ($2\hbar\omega = E_{opt}$), the transmission across a sample of thickness d is no longer described by Beer's law, but by the expression:

$$\begin{aligned} T &= \frac{1}{1+\alpha_2 dI}; \\ \alpha_2 &= \frac{N\delta}{\hbar\omega}, \end{aligned} \tag{2.37}$$

where α_2 is the TPA coefficient, N the density of molecules, δ the TPA cross section, and I the irradiance. Multiphoton absorption processes have been used to expand the range of wavelengths and conditions of illumination under which a material displays a photoconductive response (e.g. to demonstrate photorefractive polymers with non-destructive readout and operating at near-infrared wavelengths [108–111]).

Regardless of the mechanism, the photogeneration of free carriers in a solid leads to a change in the density of holes and electrons. Under steady-state conditions the total density of carriers can be expressed as:

$$\begin{aligned} n &= n_{dark} + \Delta n = n_{dark} + G_n(\hbar\omega)\tau_n, \\ p &= p_{dark} + \Delta n = p_{dark} + G_p(\hbar\omega)\tau_p, \end{aligned} \tag{2.38}$$

where $G_{n,p}$ is the generation (in this case, photogeneration) rate of electrons (holes) per unit time and volume, and $\tau_{n,p}$ is the average lifetime of electrons (holes), defined as:

$$\begin{aligned} \tau_n(t) &= \frac{\Delta n}{\partial \Delta n(t)/\partial t} = \frac{\Delta n}{R_n}, \\ \tau_p(t) &= \frac{\Delta p}{\partial \Delta p(t)/\partial t} = \frac{\Delta p}{R_p}, \end{aligned} \tag{2.39}$$

where $R_{n,p}$ is the recombination rate of excess carriers. Note that in general this recombination rate can arise from one or more physical processes. Some of the most important recombination processes will be described in the next section.

A change in carrier density will lead to the emergence of quasi-Fermi levels and to the generation of an electrical current. In addition, a change in carrier density can also lead to a change in charge carrier mobility. Therefore, the most general expression describing the change in conductivity produced in a solid under photoexcitation is given by the differential change of the conductivity:

$$\begin{aligned}\sigma_{\text{photo}} &= q\big(\Delta n\mu_n + \Delta p\mu_p + n\Delta\mu_n + p\Delta\mu_p\big) \\ &= q\big(G_n(\hbar\omega)\tau_n\mu_n + G_p(\hbar\omega)\tau_p\mu_p + n\Delta\mu_n + p\Delta\mu_p\big).\end{aligned} \tag{2.40}$$

The total conductivity is then given by: $\sigma = \sigma_{\text{dark}} + \sigma_{\text{photo}}$ and the current density can thus be separated as: $\mathbf{j} = \mathbf{j}_{\text{dark}} + \mathbf{j}_{\text{photo}}$.

The product $\mu\tau$ in Eq. (2.40) represents an important metric of a photoconductor since it determines the fraction of carriers that can be collected in an external circuit and give rise to the definition of the so-called photoconductive gain factor $g_{\text{pc},n,p}$ as:

$$\tau_{n,p}\mu_{n,p}(F) = \frac{\tau_{n,p}}{\tau_{\text{transit},n,p}}\frac{d}{F} = g_{\text{pc},n,p}\frac{d}{F}, \tag{2.41}$$

where we have defined the transit time as $\tau_{\text{transit},n,p} \equiv d\big(F\mu_{n,p}(F)\big)^{-1}$.

In steady-state and under continuous monochromatic illumination, the generation rate is proportional to the rate of absorbed photons:

$$G_{n,p}(\hbar\omega) = \eta_{n,p}(\hbar\omega)g_{\text{pc},n,p}\frac{(1-R(\omega))}{\hbar\omega}\frac{dI(\omega,z)}{dz}, \tag{2.42}$$

where $\eta_{n,p}$ is the quantum yield or photogeneration efficiency of electrons (holes), R is the reflectance, and $I(\omega,z)$ the incident irradiance. The product $\phi_{\text{int}} \equiv \eta_{n,p}$ $g_{pc,n,p}$ is commonly referred to as the internal photogeneration efficiency, and ϕ_{ext} $\equiv \phi_{\text{int}}(1-R)dI/dz$ is referred to as the external quantum efficiency.

Technologically relevant photoconductors are good insulators in the dark and become good conductors under illumination, thus another common metric used to assess a photoconductor performance is the photosensitivity, defined as:

$$\text{Photosensitivity} = \frac{\sigma_{\text{photo}}}{\sigma_{\text{dark}} + \sigma_{\text{photo}}}. \tag{2.43}$$

This factor is particularly important in the context of photorefractive materials since the space-charge field is proportional to this factor [112]. Other figures of merit often used to assess the performance of a photoconductor are $\sigma_{\text{photo}}/\alpha$, where α is the absorption coefficient, and σ_{photo}/I.

2.7.1.1 Approximations in the Context of Photorefractive Materials

In the context of photorefractive materials the following considerations should be taken into account: (1) transport is typically unipolar; (2) samples are sufficiently thick so that thin-film interference effects can be neglected and the transmittance across the film is well described by Beer's law: $I(\omega, z) = I_0 \exp(-\alpha z)$, where α is the absorption coefficient. The photogeneration rate can then be expressed as:

$$G(\hbar\omega) = \phi_{\text{int}}(\hbar\omega)(1 - R(\omega))\frac{\alpha(\omega)I(\omega, z)}{\hbar\omega}; \tag{2.44}$$

(3) absorption is weak across the sample thickness so the photogeneration can be considered uniform and the average transit time per photogenerated carrier is $\tau_{\text{transit}}/2$; and (4) the photorefractive sample is biased through blocking contacts, so injection of carriers is neglected. Under these approximations the photoconductivity can be expressed as [113]:

$$\sigma_{\text{photo}} = \phi_{\text{int}}\frac{q\alpha dI}{2F\hbar\omega}(1 - R). \tag{2.45}$$

Finally it should be noted that the presence of trapping sites is introduced into this formalism through Eq. (2.39) by realizing that the carrier lifetime is inversely proportional to the recombination rate, which, as we will later describe is proportional to the initial density of traps, T_i, and free carriers [114]. The following section presents some fundamental aspects of the photogeneration processes in organic semiconductors by reviewing current understanding of exciton dissociation on intrinsic and extrinsic organic semiconductors.

2.7.1.2 Exciton Dissociation

Neutral excitons are the precursors for the generation of free charge carriers in any semiconductor. In amorphous organic semiconductors, Frenkel excitons are strongly bound and consequently exciton dissociation is severely impaired. This leads to a common scenario where photogeneration of free carriers is attained by means of a field-assisted reduction of the ionization energy for two charges bound by their mutual Coulomb attraction. As originally described by Frenkel [75], the field-assisted reduction of the potential barrier in a Frenkel exciton is given by

$$\Delta U = \sqrt{\frac{q^3 F}{\pi\varepsilon_0\varepsilon}}. \tag{2.46}$$

Consequently, and in contrast with inorganic semiconductors displaying Wannier excitons, the photogeneration efficiency in an organic amorphous semiconductor is strongly field-dependent.

Although applying an external electric field is a common approach to overcome the exciton binding energy and to assist the photogeneration of free carriers, a large number of other possible scenarios exist that could result in the dissociation of excitons. For instance, among other processes, dissociation of excitons can occur via [115, 116] (a) dissociation at an electrode/semiconductor or semiconductor/semiconductor interface, (b) dissociation due to the interaction with trapped carriers, (c) dissociation due to a complete electron transfer taking place in intermolecular charge transfer complexes, or (d) an autoionization via intramolecular charge transfer between donor and acceptor moieties of a molecule. Such processes can be classified as intrinsic (d) or extrinsic (a–c).

2.7.1.3 Photogeneration in Intrinsic Photoconductors: Onsager Model

Photogeneration in intrinsic photoconductors has been successfully described by the geminate recombination theory developed by Onsager [117]. Onsager's model is based on the assumption that charge photogeneration occurs via thermal dissociation of an intermediate charge state resulting from the thermalization of an exciton and leading to the formation of an electron–hole pair held by its Coulomb attraction (geminate pair) and having a field-dependent probability of dissociation $P(r, F, T)$, as shown in Fig. 2.4.

The dissociation probability of the geminate pair is found using Smoluchowski diffusion equation [118] to describe the Brownian motion of the geminate pair under its Coulomb potential and under an externally applied electric field. If the pair separation reaches zero, the model considers that the pair disappears undergoing geminate recombination. Under this assumption the photogeneration efficiency is calculated as

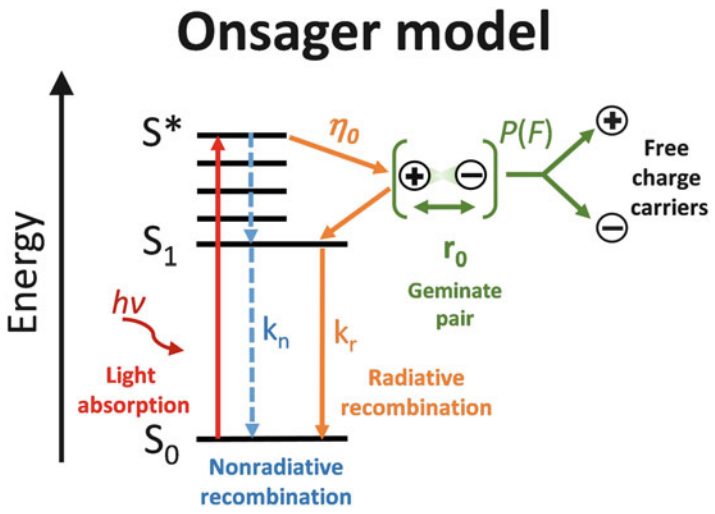

Fig. 2.4 Onsager model for charge generation

$$\eta(r,F,T) = \eta_0 \int 4\pi r^2 P(r,F,T) f(r) dr, \tag{2.47}$$

where η_0 is the quantum yield, i.e. the fraction of absorbed photons that results in a thermalized geminate pair, $P(r, E, T)$ is the dissociation probability of geminate pairs separated by a distance r under an electric field E and at a temperature T, and $f(r)$ is the initial spatial distribution of the geminate pairs. The integral can be simplified if it is assumed that the spatial distribution of the pairs is spherically symmetrical and that all pairs are separated by the same distance r_0 after being thermalized, hereafter known as the thermalization length. Therefore, by assuming $f(r) = (4\pi\, r^2)^{-1}\delta(r - r_0)$ the photogeneration efficiency is reduced to $\eta = \phi_0 P(r_0, F, T)$. The dissociation probability was approximated numerically by Mozumder [119] and the following expression for the photogeneration efficiency derived:

$$\begin{aligned} \eta(r_0,F,T) &= \eta_0 \left[1 - \zeta^{-1} \sum_{n=0}^{\infty} A_n(\kappa) A_n(\zeta) \right] \\ \zeta &= \frac{q r_0}{kT} F, \quad \kappa = \frac{R_c}{r_0}, \quad R_c = \frac{q^2}{4\pi\varepsilon_0 \varepsilon_r kT}, \end{aligned} \tag{2.48}$$

where the coefficients $A_n(x)$ are defined through the recursive relations

$$\begin{aligned} A_n(x) &= A_{n-1}(x) - \frac{x^n \exp(-x)}{n!}, \\ A_0(x) &= 1 - \exp(-x). \end{aligned} \tag{2.49}$$

This numerical approximation requires the first 10–20 terms to provide good convergence [119].

2.7.1.4 Photogeneration in Extrinsic Photoconductors

Solids wherein donor and acceptor molecules form strong charge transfer states represent one of the most common approaches towards improving the photogeneration efficiency of photorefractive polymers in particular, and of organic photosensitive materials in general. Onsager's model fails to predict the photogeneration process in such extrinsic photoconductors, leading to unreasonably large thermalization lengths (2–3 nm) inconsistent with the nearest-neighbor electron transfers expected from spectroscopic studies, where typical intermolecular distances are ca. 0.5 nm [120]. These discrepancies were recognized and addressed by Noolandi and Hong [121] and later by Braun [120], who developed a kinetic model that identified the geminate pairs with an electron transfer state having a finite lifetime (ca. nanosecond range), and formed by direct optical excitation, or when a neutral donor (acceptor) excited state encounters an acceptor (donor) in its ground state. Both models recognized the unrealistic assumption of an instantaneous

recombination rate assumed in Onsager's model by requiring annihilation of a geminate pair at zero distance. The recombination process requires the dissipation of energy into the vibrational modes of the material, which cannot happen instantaneously. A weakness in all models, already recognized by Noolandi and Hong, is the assumption of field independent rates for the creation and recombination of geminate pairs. An attempt to develop a model that incorporated semiclassical electron transfer theories developed by Marcus [122, 123] for the description of such rates was introduced by Wang and Suna [124] for the case of a classical photoconductor consisting of PVK doped with fullerene molecules. This new model addressed the diffusion of a charge pair in terms of a pair distribution function $\rho(\mathbf{r})$ by considering the current describing the separation of holes and electrons as

$$\mathbf{j}(\mathbf{r}) = -D\left(\nabla\rho(\mathbf{r}) + \frac{q}{kT}\nabla V(\mathbf{r})\rho(\mathbf{r})\right), \tag{2.50}$$

where D is Einstein diffusion constant and $V(\mathbf{r})$ is the potential considering the Coulomb interaction between the electron–hole pair and the external electric field, F_0:

$$V(\mathbf{r}) = -\frac{q}{\varepsilon_0\varepsilon|\mathbf{r}|} - F_0 z. \tag{2.51}$$

Conservation of particles leads to a steady-state transport equation for the pair distribution, given by

$$\nabla \cdot \mathbf{j}(\mathbf{r}) = \beta(\mathbf{r})\rho(\mathbf{r}) + s(\mathbf{r}), \tag{2.52}$$

where $\beta(\mathbf{r})$ is the electron–hole recombination rate at $\mathbf{r}$, $s(\mathbf{r})$ the rate of pair creation at the same position, proportional to the rate of creation of excited states, s_0. Expressions for β and s are then derived using Marcus theory [122, 123]. The photogeneration efficiency thereafter is obtained as the ratio of charge flux escaping to infinity to the excited state creation rate:

$$\eta = \frac{1}{s_0}\int_{\Omega} \mathbf{j}(\mathbf{r}) \cdot \mathbf{n}\, d^2 r, \tag{2.53}$$

where $\mathbf{n}$ is the normal vector to the surface Ω, enclosing all of the excited states. Good agreement with the experimental data was obtained using this model [124], but need for a complex numeric approach limits its applicability.

2.7.1.5 Empirical Approximations

Although models for the field-dependent photogeneration in extrinsic photoconductors are based on more realistic assumptions than the simpler Onsager model, the complexity of these numerical solutions results less attractive than

approximating the field-dependent photogeneration efficiency by an empirical expression of the form [102, 125, 126]:

$$\eta(F) = s_0 F^p, \tag{2.54}$$

where s_0 is the photogeneration cross section and p a constant determined experimentally with values typically between 1.5 and 3.5 [127]. This expression is valid in the range from ca. 10 to 100 V/μm, but the physical insight into the photogeneration process is lost following this approach.

2.8 Recombination

Electrons in the conduction band and holes in the valence band can recombine if they come too close to each other to escape their mutual Coulomb attraction. In a recombination event, an electron in the conduction band losses its energy *via* two possible pathways: optically, by radiative recombination resulting in the emission of a photon, or thermally, by nonradiative recombination.

At thermal equilibrium, and in the absence of external electric fields, electrons in the conduction band, or holes in the valence band, move randomly until they recombine, thus maintaining charge neutrality and implying that the rate of generation of carriers, G, must be equal to the recombination rate, R.

Since a recombination event involves one electron and one hole, it is also described as bimolecular recombination, and is calculated through the general expression:

$$R = \gamma(n_c p_v - n_i p_i) \approx \gamma n_c p_v, \tag{2.55}$$

where γ is known as the recombination rate constant. Figure 2.5 summarizes some of the relevant recombination mechanisms that will be briefly described in the remainder of this section.

2.8.1 Langevin Recombination Theory

Langevin's theory [128] describes bimolecular recombination as the likelihood that opposite charge carriers find each other. In three dimensions, the recombination rate is determined by diffusion and drift of a hole and an electron under its Coulomb attraction. Recombination occurs if the hole and electron reach a critical distance

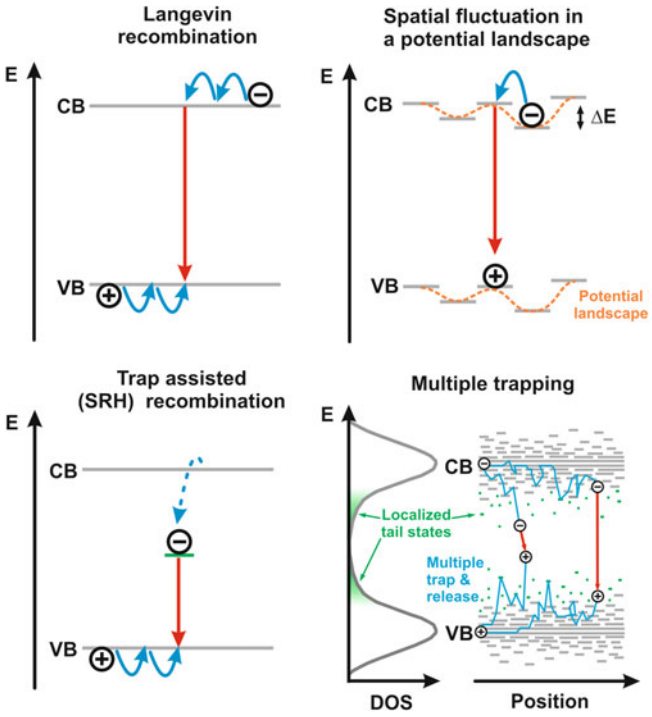

Fig. 2.5 Schematics of recombination mechanism discussed in this section

defined by the Coulomb capture radius or Onsager radius, R_C, defined as the radius where the thermal and electrostatic energies are equal:

$$R_C(T, \varepsilon_r) = \frac{q^2}{4\pi\varepsilon_0\varepsilon_r kT}, \tag{2.56}$$

where $\varepsilon_0 = 8.85 \times 10^{-12}\,\mathrm{F/m}$ is the electric permittivity of vacuum and ε_r is the dielectric constant of the medium. At room temperature, $T = 300$ K, $R_C(300K, \varepsilon_r) = 55.6\,\mathrm{nm}/\varepsilon_r$. Organic semiconductors typically display ε_r values of ca. 2–4, leading to typical Coulomb capture radius in the range between 14 and 28 nm, often slightly reduced by energetic disorder but nonetheless significantly larger than the ones obtained in inorganic semiconductors, for instance, in Si, $R_C(300K, 11.7) = 4.8\,\mathrm{nm}$.

The recombination rate constant according to Debye-Smoluchowski theory is given by:

$$\gamma_{SM} = 4\pi R_C\left(D_n + D_p\right). \tag{2.57}$$

Assuming the validity of Einstein relation (i.e., at low carrier concentrations and low electric fields [68, 69]), Eq. (2.57) leads to the expression:

$$\gamma_{\mathrm{LAN}} = \frac{q}{\varepsilon_0 \varepsilon_r}\left(\mu_n + \mu_p\right) = \frac{q\mu}{\varepsilon_0 \varepsilon_r}, \tag{2.58}$$

where μ is the relative mobility at which electrons and holes come together (i.e., if we assume one of the carriers is fixed and the other one is moving). Equation (2.58) is the result obtained using the Langevin formalism. It should be noted that implicit in this formalism are two important assumptions: (1) that the mean-free path of charge carriers is smaller than R_{C}, a condition that is well satisfied in disordered organic semiconductors where charge transport occurs by hopping events and (2) that the electron and hole densities are uncorrelated and homogeneous across the material. The latter condition is not necessarily fulfilled in disordered organic semiconductors where the densities are correlated by electronic localization and can lead to significant distortions of the local charge density around a free charge. Although the Langevin theory has proven successful in the context of crystalline semiconductors including organic crystals [129], where the density of hole and electrons are similar and uncorrelated; and in amorphous materials at the zero-carrier density limit [130] (e.g. for electric fields up to ca. 50 V/μm and energetic disorder up to ca. 0.25 eV), this volumetric description typically fails to describe systems with lower dimensionality [131, 132] or systems where charge transport is highly inhomogeneous across a device such as in bulk-heterojunction OPV.

2.8.1.1 Spatial Fluctuation in a Potential Landscape

A model to describe bimolecular recombination in disordered semiconductors was proposed by Adriaenssens and Arkhipov [133] by taking into account spatial charge profiles and energetic disorder but assuming the carrier localization radius to be smaller than the characteristic length of these spatial fluctuations. In this scenario, the recombination rate constant determined by the Langevin theory is modified by a thermally activated term, with an activation energy barrier, Δ_{E}, defined as the characteristic amplitude of the potential fluctuations.

$$\gamma = \frac{2\pi}{kT}\Delta_{\mathrm{E}}\exp\left(-\frac{2\Delta_{\mathrm{E}}}{kT}\right)\gamma_{\mathrm{LAN}}. \tag{2.59}$$

2.8.1.2 Trap-Assisted Recombination

The presence of deep traps in a semiconductor immobilizes electrons or holes and facilitates recombination with mobile carriers. This, two-step process, is known as trap-assisted recombination and is commonly referred to as Shockley-Read-Hall

(SRH) recombination. If we assume that traps with energy E_T exist in a semiconductor, the trapping rate in steady-state is given by:

$$\begin{aligned} R_{SRH} &= \frac{np - n_1 p_1}{C_n(n + n_1) + C_p(p + p_1)}, \\ n_1 &\equiv N_c \exp\left(\frac{E_T - E_c}{kT}\right), \\ p_1 &\equiv N_v \exp\left(\frac{E_v - E_T}{kT}\right), \end{aligned} \tag{2.60}$$

where $C_{n,p}$ are the probabilities per unit time that an electron or hole, respectively, will be captured under the assumption that all traps are empty, and n_1 and p_1 are the electron and hole densities when the Fermi level equals the trapping level.

2.8.1.3 Multiple Trapping–Detrapping

In the context of bulk heterojunction OPV, Nelson [134] proposed a model for charge recombination where the rate is limited by the diffusion of polarons having a DOS containing a tail of deep traps. In the context of the multiple trapping model, diffusion is mediated by multiple trapping and release events from a population of deep traps. Trapping makes the recombination rate dependent only on the density of free polarons, p_{free}, instead of the total density, p_v, resulting in the modified expression:

$$R = \gamma n_c p_{free}. \tag{2.61}$$

2.9 Photoconductivity and Space-Charge Field Formation in Photorefractive Polymers

The models of charge transport herein described have been adapted to describe the formation of space-charge fields in photorefractive polymers using the drift-diffusion model.

2.9.1 Space-Charge Field: Steady-State

The first comprehensive theoretical model for the formation of space-charge fields in a photorefractive material was introduced by Kukhtarev and coworkers [135, 136]. The model used rate equations to describe charge redistribution on a wide gap semiconductor with a single impurity level subjected to a periodical

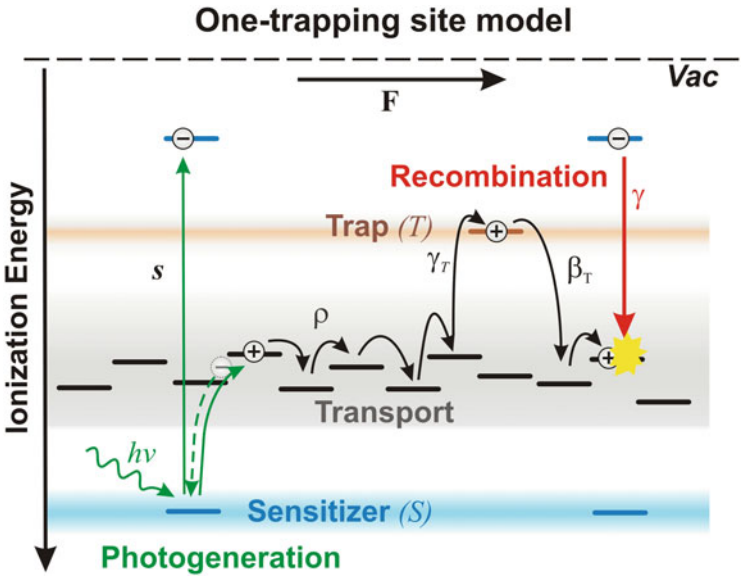

Fig. 2.6 Physical processes considered in Schildkraut's one-trapping site model for a hole transporting polymer

irradiance distribution. Kukhtarev's model produced good agreement with experimental results obtained on inorganic photorefractive crystals and became widely accepted.

The first model for the formation of space-charge fields in the context of photorefractive polymers was presented by Schildkraut and coworkers [125, 126]. Schildkraut's model can be considered a direct analog of Kukhtarev's model in the sense that a single trapping level and unipolar charge transport are assumed. A schematic representation of the physical processes considered in Schildkraut's model is given in Fig. 2.6. Free-holes are assumed to be photogenerated *only* through photon absorption in a sensitizer molecule. Photogenerated holes in the transport manifold can either recombine, at a rate γ, with sensitizer anions to produce neutral sensitizer molecules or become trapped at a rate γ_T, and thermally detrapped at a rate β_T. In Schildkraut's original paper the recombination and trapping rates were assumed to follow Langevin theory, this is, to be dominated by the strong Coulomb attraction between carriers of opposite sign. In organic photoconductors wherein the photogeneration of carriers arises exclusively through sensitizer molecules, recombination exclusively involves the annihilation of a free charge with an immobile ionized sensitizer.

The modified set of nonlinear equations describing the space-charge field dynamics in Schildkraut's model is given by

$$\begin{aligned}
\frac{\partial \rho}{\partial t} &= \frac{\partial S^-}{\partial t} - \frac{\partial T^+}{\partial t} - \frac{1}{q}\frac{\partial J}{\partial x}, \\
\frac{\partial F}{\partial x} &= \frac{q}{\varepsilon_0 \varepsilon}(\rho + T^+ - S^-), \\
\frac{\partial T^+}{\partial t} &= \gamma_T (T - T^+)\rho - \beta T^+, \\
\frac{\partial S^-}{\partial t} &= sI(S - S^-) - \gamma S^- \rho, \\
J &= q\mu\rho F - qD\frac{\partial \rho}{\partial x},
\end{aligned} \tag{2.62}$$

where ρ is the free charge (hole or electrons) density, J is the current density, S and T the total density of sensitizers and traps, respectively, S^- the density of sensitizer anions, T^+ the density of filled traps, μ is the mobility, D is Einstein's diffusion coefficient, I is the irradiance, and s the photogeneration cross section.

Herein, no assumptions have been made with respect to the functional form of the field dependence of the trapping, detrapping, and recombination rates. Schildkraut incorporated a field dependent photogeneration efficiency, mobility, recombination, and trapping rates using the following approximations:

$$\begin{aligned}
\eta(F) &= \eta_i F^A, \\
\mu(F) &= \mu_0 \exp\left\{C\left[\sqrt{F} - \Delta_0/B\right]\right\},
\end{aligned} \tag{2.63}$$

where Δ_0 is the activation energy and η_i, A, B, and C are constants determined experimentally. These functional forms have been shown to be reasonable approximations for electric fields in the range between 10 and 100 V/μm [76, 120, 125, 126].

In the limit of low absorption, when the free-hole density is much smaller than the trap density, the photogeneration efficiency and cross section are related through the equation:

$$\eta(F) = S^- \frac{\hbar\omega}{\alpha(\omega)} s(F), \tag{2.64}$$

where α is the absorption coefficient, $\hbar$ is the Planck constant, ω the light frequency, and S^- the steady state concentration of ionized sensitizer molecules.

In the context of photorefractive polymers, Eq. (2.62) has been linearized to obtain steady-state solutions of the space-charge field. Solutions are described in [114, 125].

2.9.1.1 Space-Charge Field: Temporal Evolution

Schildkraut's model has also been used to describe the temporal evolution of the space-charge field in certain limiting cases for the grating erasure process in a material containing: (a) no traps; (b) deep inactive traps (no detrapping); (c) deep traps but allowing optical detrapping; and (d) shallow traps; as well as to describe transient photoconductivity measurements [102, 137]. An analytical solution of the first-order Fourier component of the space-charge field was derived by Cui and coworkers [138]. Using a similar approach, Yuan and coworkers derived a kinetic differential equation for the formation of the space-charge field as a function of the light intensity and the grating spacing, first for the case of no trapping, and in later papers [139–142] for the cases of deep traps (high and low density) and to consider moving gratings driven with a periodic force at an arbitrary frequency. Besides the restricted experimental situations where the models are valid, the static and dynamic solutions of the models all share a common limitation in that a large number of material parameters need to be known before any quantitative evaluation can be made. Information about the mobility, the photogeneration efficiency, trapping and detrapping rates is required and not always easy to gather experimentally with existing techniques. However, it has also been demonstrated that a systematic analysis of the temporal dependence of the photoconductive properties of a photorefractive material yields enough information to describe the dynamic evolution of the space-charge field. This approach was first presented by Ostroverkhova and Singer [102] and later modified by Kulikovsky and coworkers [106].

Figure 2.7 depicts the physical processes considered by Ostroverkhova and Singer to expand the one-trapping site approach proposed by Schildkraut by considering

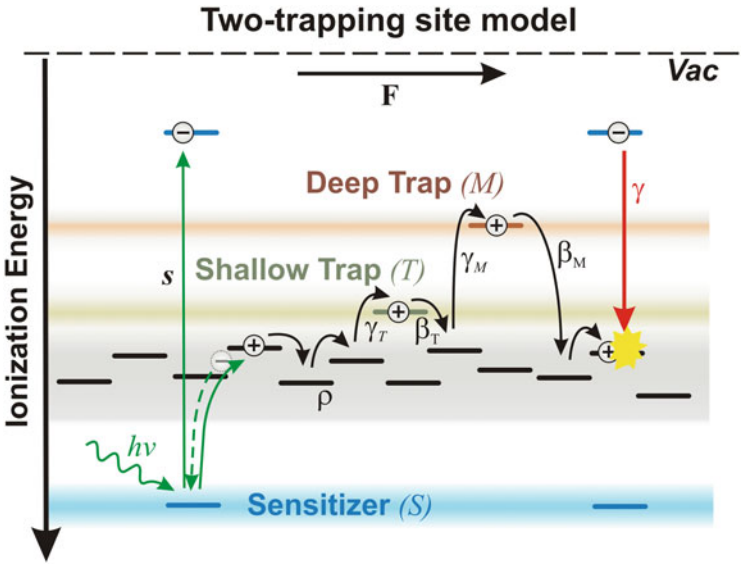

Fig. 2.7 Schematic representation of charge redistribution in the two-trapping site model

the more realistic situation of having at least two well-defined trapping levels: one regarded as a deep trapping level, already considered in Schildkraut's work, and a second regarded as a shallow trapping level; a situation already observed experimentally in a variety of photorefractive polymers [26, 82, 113, 138, 143].

The modified set of nonlinear equations considered by Ostroverkhova's model is written as:

$$\begin{aligned}
\frac{\partial \rho}{\partial t} &= \frac{\partial S^-}{\partial t} - \frac{\partial T^+}{\partial t} - \frac{\partial M^+}{\partial t} - \frac{1}{q}\frac{\partial J}{\partial x}, \\
\frac{\partial F}{\partial x} &= \frac{q}{\epsilon_0 \varepsilon}(\rho + T^+ + M^+ - S^-), \\
\frac{\partial T^+}{\partial t} &= \gamma_{\mathrm{T}}(T - T^+)\rho - \beta_{\mathrm{T}} T^+, \\
\frac{\partial M^+}{\partial t} &= \gamma_M (M - M^+)\rho - \beta_M M^+, \\
\frac{\partial S^-}{\partial t} &= sI(S - S^-) - \gamma S^- \rho, \\
J &= q\mu\rho F - qD\frac{\partial \rho}{\partial x},
\end{aligned} \tag{2.65}$$

where T and M are the total density of shallow and deep traps, respectively; T^+ and M^+ the density of filled shallow and deep traps, respectively; β_{T} the thermal shallow-trap detrapping rate; and β_M the thermal deep-trap detrapping rate. The rest of the parameters are defined as above. In contrast with previous models, the thermal detrapping rate for the deep traps is considered non-zero but required to be at least one order of magnitude smaller than that of the shallow traps. Following a Fourier decomposition approach, Eq. (2.65) can be separated in those governing the zero-order (uniform illumination) and first-order (spatially varying illumination) parameters. The zero-order system of equations describing the temporal evolution under uniform illumination is given by:

$$\begin{aligned}
\rho_0(t) &= S_0^-(t) - T_0^+(t) - M_0^+(t), \\
\frac{\partial T_0^+(t)}{\partial t} &= \gamma_{\mathrm{T}}(F_0)\left[T - T_0^+(t)\right]\rho_0(t) - \beta_{\mathrm{T}} T_0^+(t), \\
\frac{\partial M_0^+(t)}{\partial t} &= \gamma_M(F_0)\left[M - M_0^+(t)\right]\rho_0(t) - \beta_M M_0^+(t), \\
\frac{\partial S_0^-(t)}{\partial t} &= s_0(F_0) I_0\left(S - S_0^-(t)\right) - \gamma(F_0) S_0^-(t)\rho_0(t), \\
J(t) &= q\mu_0(F_0)\rho_0(t) F_0.
\end{aligned} \tag{2.66}$$

Further simplification of this system of equations can be made to consider the limiting situations for a trap-unlimited regime ($S \ll T, M$) or a trap-limited regime (i.e., $M < S < T$). In any case, this system of equations can be solved numerically for $\rho_0(t)$, $T_0^+(t)$, $M_0^+(t)$, $S_0^-(t)$ if the relevant rates are known. All the parameters relevant for the description of the temporal evolution of the space-charge field can be obtained through time resolved photoconductivity experiments. Knowledge of zero-order components allows solving numerically for the temporal evolution of the first-order components as described by Schildkraut [126].

The models herein presented are limited to low electric fields (less than 50 V/μm) because effects such as grating bending [144], grating fanning [145], grating competition [146], and effects of chromophore reorientation in the formation of the photorefractive gratings [147] are not described within this formalism, but are nonetheless commonly encountered. Despite limitations, current models offer already important insight into factors affecting the space-charge field strength and build-up speed. In particular, these models suggest that to improve the dynamic response of photorefractive materials, significant improvements on the charge carrier mobility and photogeneration efficiency values displayed by these materials will have to be achieved.

Over the last decade, remarkable progress has been made towards the development of a new breed of organic semiconductors, forcing a reevaluation of preconceived notions on how to optimize charge transport and photogeneration in disordered organic semiconductors and opening exciting new routes for the optimization of organic optoelectronic devices. The following section provides a short review of progress made in the development of novel organic semiconductors.

2.10 Materials

Until recently, the development of organic molecules has followed well-defined guidelines: (1) prescence of accessible π-electron groups that facilitate intermolecular π–π overlap; (2) molecular planarity and rigidity to achieve low reorganization energy values, to reduce the formation of lattice defects, and to minimize thermal fluctuations (which contribute to charge localization and energetic disorder); and (3) molecular packing configurations that lead to strong intermolecular electronic coupling. These guidelines have favored development of organic semiconductors which display a high degree of crystallinity and highly anisotropic charge transport characteristics. For instance, crystals of unsubstituted π-conjugated molecules (e.g., acenes such as pentacene, and oligothiphenes) typically display a layered herringbone packing which leads to 2D transport within the stacked layers and reduced transport within single layers [36]. In this context, control over molecular packing has represented one of the most important aspects for the optimization of transport in organic semiconductors. However, development of design rules and processing techniques that allow control over intermolecular packing and over the formation of energetic and structural defects remains a challenging task.

State-of-the-art crystalline organic semiconductors based on acenes and benzothiophenes display charge mobility values in the range from ca. 10 to 40 cm^2/Vs, while amorphous organic semiconductors display values well below 0.1 cm^2/Vs. In this context, it is worth pointing out that organic photorefractives are typically classified as amorphous semiconductors. This is because the most common approach towards producing organic photorefractives has been to blend: (1) a host molecule (i.e., a polymer) providing the main charge transport manifold; (2) plasticizer molecules to reduce the glass transition temperature, T_g, of the composite; (3) sensitizer molecules to provide charge generation at the desired wavelength by facilitating a photoinduced charge-transfer reaction to the molecular host; and (4) chromophores to confer electro-optic (EO) properties to the mixture. This approach typically results in highly disordered semiconductors that display mobility values well below 10^{-4} cm^2/Vs.

In recent years, a new breed of organic semiconductors based on molecules displaying donor–acceptor molecular complexes has been developed. These novel materials can neither be classified as amorphous or as polycrystalline since they display various degrees of order at different length scales, ranging from crystalline to completely amorphous. Seemingly amorphous semiconductors based on molecules with donor–acceptor motifs have been shown to display charge mobility values on the order of ca. 1 cm^2/Vs, and are forcing a reevaluation of existing paradigms towards molecular design and optoelectronic device optimization.

In the following sections, we will review current material approaches used in organic photorefractives as well as recent advances in the development of organic semiconductors with improved charge transport characteristics. The chemical structures of some of the most relevant molecules and molecular motifs used in state-of-the-art organic semiconductors to be discussed in the following sections are shown in Fig. 2.8.

2.10.1 Extrinsic Photoconductors

For historical reasons, photoconductive materials used in organic photorefractives have displayed primarily hole-transport properties. For this reason, electron-deficient organic molecules [14, 15, 113, 148, 149] such as fullerenes, phthalocyanines, squaraines, perylene dyes, and thiapyrylium salts, transition metal complexes [150, 151] as well as inorganic semiconductor nanocrystals [152, 153] have been used as sensitizers to produce extrinsic photoconductors operating at the spectral regions of interest [47, 48, 127]. To date, three main regions of interest exist to develop photorefractive materials depending on the application. For display applications, photoconductive materials operating in the visible spectral range, from ca. 400 to 700 nm, are needed; for biomedical applications in the near-infrared spectral range, from ca. 700 to 1100 nm; and for telecommunications in the spectral range from ca. 1300 to 1550 nm.

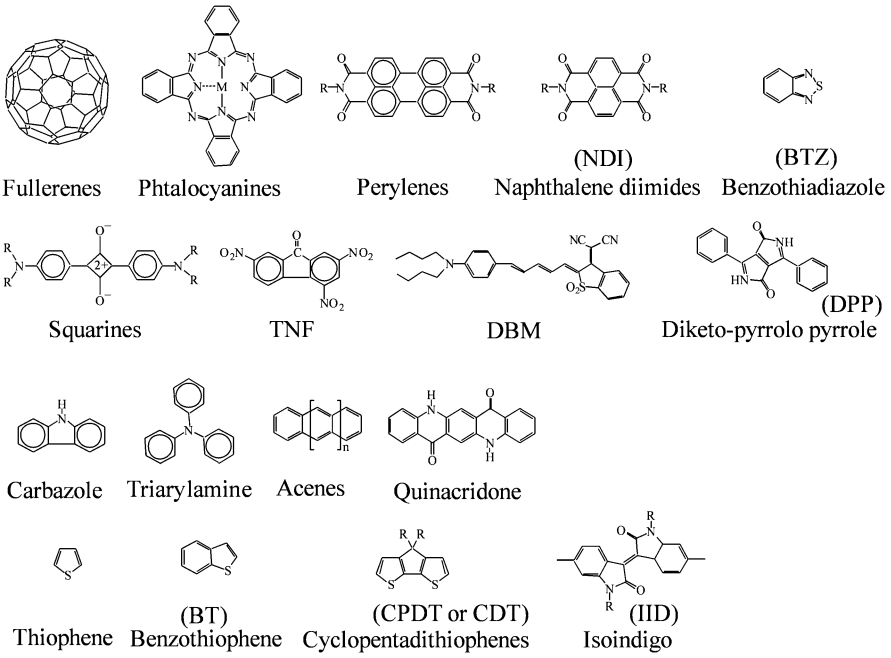

Fig. 2.8 Chemical structure of some of the most relevant molecules and molecular motifs used in state-of-the-art organic semiconductors

2.10.1.1 Sensitizers and Charge-Transfer Complexes

The development of organic photoconductors based on hole-transporting polymer owes its origin to the commercial success in xerographic applications of the extrinsic photoconductor composite comprising poly(vinylcarbazole) (PVK) and trinitrofluorenone (TNF). In this composite, the electron-donating (*D*) polymer PVK confers hole-transporting properties to the composite, while the electron-accepting (*A*) molecule TNF is used as sensitizer. TNF is chosen because strong intermolecular interactions with PVK give rise to the formation of a molecular complex known as charge-transfer (CT) complex. A CT complex exhibits new absorption bands, not present in the absorption spectrum of the isolated materials, from which the photogeneration of charge-carriers is greatly facilitated. Although photogeneration is possible through the direct photoexcitation of the transport moiety (i.e., PVK), as in the case of intrinsic photoconductors, the photogeneration efficiency values displayed by a pristine material is generally orders of magnitude smaller than values displayed by a sensitized composite due to the large exciton binding energy values found in organic materials.

The success of this approach has defined a paradigm for the development of organic photoconductors based on guest–host polymer composites wherein the donor and acceptor moieties display a strong electronic coupling leading to the

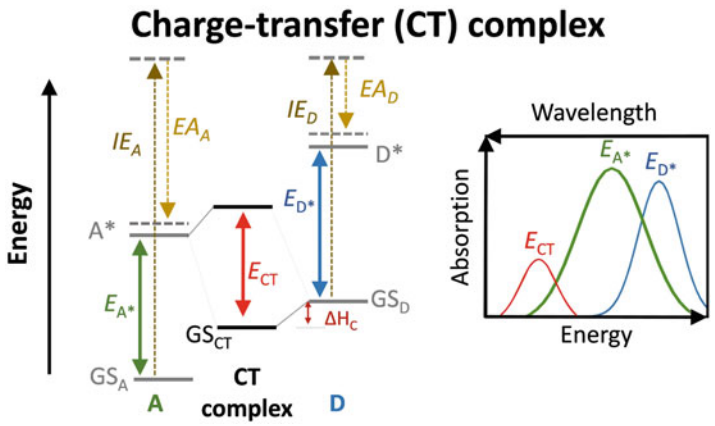

Fig. 2.9 Energy levels and schematics of absorption profiles of uncomplexed acceptor (A) and donor (D) molecules and of charge transfer state

formation of CT complexes. The formation of a CT complex is often evident from the emergence of new red-shifted spectral bands that are not present in the spectrum of the individual molecules, see Fig. 2.9, extending the spectral sensitivity of the photoconductor towards lower wavelengths. The photon energy of these new bands, characterized by the photon energy, E_{CT}, can be engineered by tailoring the ionization energy of the donor molecule, IE_D [154]. As shown in Fig. 2.9, the difference that exists between the CT ground state and the donor ground state corresponds to the enthalpy of complexation ΔH_C. According to Marcus theory, in the non-inverted regime, the rate of electron transfer from the donor to the CT state will increase with increasing ΔH_C resulting in an increased photogeneration efficiency in blends having stronger donors with smaller IE_D values. Although the detailed nature of the electronic coupling that arises between a donor and acceptor molecule in a blend can be very complex, these relations provide simple guidelines for the selection of potential donor and acceptor pairs based on the energetic properties of the isolated molecules.

2.10.1.2 Photoconductors for Photorefractive Applications I: Organic Sensitizers

The use of photoconductors based on charge-transfer complexes has been the preferred approach towards the realization of organic photorefractives. In the visible range, fullerene (C_{60}) and its derivatives, such as C_{70} and $PC_{60}BM$ [149], have been widely used as sensitizing molecules because C_{60} forms strong CT complexes with electron-rich aromatic amines, such as *N*,*N*-diethylaniline; a building block of commonly used hole transport materials such as carbazoles [148, 155]. This realization led to the demonstration of large photogeneration

efficiencies in a polymer composite comprising a blend of poly(9-vinylcarbazole) (PVK) and C_{60} [148, 155]. The enhanced photoconductive properties of the PVK/C_{60} composite were also recognized to be responsible for improved photorefractive performance and faster grating build-up times compared to commonly used photoconducting composites comprising PVK/2,4,7-trinitro-9-fluorenone (TNF) [156] or PVK/(2,4,7-trinitrofluoren-9-ylidene) malononitrile (TNFDM) [113]. In addition to the formation of charge-transfer complexes between the sensitizer and the transporting moiety, evidence of complexation between sensitizer molecules and EO chromophores was also found to be of importance for the photogeneration process and consequently, for the photorefractive response [113].

Although a direct comparison of the photoconductive properties of different photorefractive composites is challenging given the variability of experimental conditions, typical values of the photoconductivity in PVK/C_{60}-based photorefractive composites are in the range between 1 and 30 nS/cm for electric field values in the range from 40 to 80 V/μm, an order of magnitude higher than photoconductivity values found on PVK/TNFDM photorefractive composites [113]. Despite large photoconductivity values achieved in PVK/C_{60}-based photorefractive composites, a major limitation towards improving the speed of photorefractive polymers (limited to values of a few milliseconds) based on this photoconductor, was identified to be the low carrier mobility displayed by PVK, with values typically in the range between ca. 10^{-8} and 10^{-6} cm^2/Vs [157]. Other carbazole-based polymers, such as polysiloxanes with pendant carbazole groups PSX [158], have been considered as a low-T_g alternative to PVK. Although in this polymer the glass transition temperature, T_g, can be tuned (40–50 °C) by varying the spacer length of the pendant carbazole group, and mobility values are comparable to those found in PVK, in general, the use of the photoconductive matrix PSX/TNF has lead photorefractive composites with slow response times.

An alternative to carbazole-based materials was identified in derivatives of the donor molecule *N*,*N*′-diphenyl-*N*,*N*′-bis(3-methylphenyl)-(1,18-biphenyl)-4,48-diamine (TPD). TPD-based materials are known to exhibit high carrier mobility values in the range between 10^{-6} and 10^{-4} cm^2/Vs [87, 157] and lower density of traps compared to PVK-based materials [159]. TPD also has been shown to form a strong charge-transfer complex with C_{60} [154], leading to two orders of magnitude improvement in PS/TPD/C_{60} composites over the photogeneration efficiency values found on PVK/ECZ/C_{60} composites. In a photorefractive polymer composite containing poly(acrylic tetraphenyldiaminobiphenol) (PATPD)/C_{60} [104] photoconductivity values ca. 1.5 nS/cm at 40 V/μm were reported. This is, in the same range of magnitude as PVK/C_{60}-based photorefractive composites and leading to response times in the millisecond range [103, 104]. A similar PATPD/C_{60}-based photorefractive polymer composite was later found able to display fast responses times of ca. 300 μs when excited with ca. 1 ns pulses at 532 nm having a total fluence of 4 mJ/cm^2 [30]. PATPD-based photorefractive polymers have also been synthesized with the near infrared dye 2-[2-{5-[4-(di-*n*-butylamino)phenyl]-2,4-pentadienylidene}-1,1-dioxido-1-benzothien-3(2*H*)-ylidene]malononitrile (DBM),

to enable this polymer composite to display photoconductivity values at 975 nm of ca 1.0 nS/cm at 56 V/μm and response times ca. 100 ms [160]. Similar PATPD/DBM-based photorefractive polymers were also shown able to display a photoconductive response at 1550 nm, by exploiting the large TPA cross section of DBM, and a fast photorefractive response of ca. 35 ms when excited with 130 fs pulses with a pulse energy of 11.4 μJ focused onto a spot with diameter ca. 180 μm [111].

It is worth noting that sensitization using a TPA process yields photoconductors that display no linear absorption and consequently no photoconductive response through one-photon absorption (thus overcoming the transparency/absorption tradeoff), but a high photoconductive response through TPA. In the first demonstration of a TPA sensitized photorefractive polymer, Blanche and co-authors demonstrated that a photoconductor comprising PVK and the chromophore FTCN displayed a diffraction efficiency of 0.03 % with buildup times on the order of seconds when excited with 150 fs pulses at 620 nm. In addition, using this approach, nondestructive readout was also demonstrated thanks to the absence of one-photon absorption, and consequently, one-photon photogeneration during readout [108, 109].

Other high performance TPD-based photorefractive polymers have been reported in the literature [149, 161–164]. However, despite displaying higher mobility values than carbazole-based polymers, the photorefractive response time of TPD-based photorefractive polymers has remained in the millisecond range. This is in part because these materials either displayed limited photoconductivity values in the range <1 nS/cm or small trap densities, required for the fast formation of a space-charge field.

In addition to TPD-polymers, small-molecule bifunctional TPD derivative 4-dicyanovinylaniline (DCVA) sensitized by C_{60} has been shown to form a stable molecular photorefractive glass with photoconductive values ca. 2 nS/cm and response times ca. 30 ms [165].

Graphene and carbon nanotubes (CNTs) have both been used as sensitizers in organic photorefractives. Graphene, in particular, is attractive because it provides a spectrally flat absorption across the visible and near infrared spectral ranges. Photorefractive polymers with a high glass transition temperature for operation at 1064 nm have been reported in PVK/graphene [166] and aromatic polyimides doped with CNTs [167]. The photorefractive properties at 633 nm of PVK-based photorefractive composites doped with CNTs and PVK grafted CNTs were also reported [168]. Common problems found in these works arise from a low contrast between the dark and photocurrent density values as well as from optical scattering, which severely hindered the photorefractive response of the material. A comparison of the photorefractive properties at 633 nm of PATPD doped with graphene and PCBM at 0.03 wt% were also reported recently. At this small loading ratios, a high contrast between the dark and photoconductivity was found, with photoconductivity values in the range of 10 pS/cm and dark conductivity values ca. 0.025 pS/cm at ca. 50 V/μm. Graphene-doped composites displayed a slight improvement in photoconductivity values and response times (in the seconds range) compared to PCBM-doped composites [169].

Phthalocyanines have also shown promising photoconductive properties as dopants of PVK. PVK-SiPc-based photorefractive polymers display photoconductivity values of 3 pS/cm at 22 V/μm and grating build-up times around 100 ms [170]. Most encouraging, the photoconductivity values of PVK/SiPc were found to be higher than those found in PVK/C_{60} within the voltage range analyzed, and for concentrations that are two orders of magnitude lower than the ones used in PVK/C_{60} composites, thus, leading to photorefractive polymers with smaller absorption coefficient values. Moreover, a Ni-dithiolene complex has also been used to extend the sensitivity of PF6TPD-based photorefractive composites into the near IR, providing sensitization at 1064 nm [171].

2.10.1.3 Photoconductors for Photorefractive Applications II: Inorganic Sensitizers

Inorganic nanoparticles have also attracted significant attention as sensitizers of organic semiconductors. This is because quantum confinement effects allow the optical and electrical properties of the semiconductor nanoparticles (quantum dots) to be engineered by controlling their size [172]. Quantum confinement effects become dominant when the size of the nanocrystals is in the same order of magnitude as the exciton Bohr radius. In the presence of quantum confinement effects, the bands can no longer be considered a continuum of states but must be regarded as discrete sets. Control over the surface of the nanoparticles is of particular importance because disruption of the boundary conditions imposed by the end of the periodicity yields electronic states within the optical bandgap, with the potential of acting as traps. Passivation of the nanoparticle surface is thus a critical step in which the surface atoms are bonded to those of another material, having a bigger bandgap than the nanocrystal. This process yields no surface states within the optical bandgap and confines the electrons and holes inside the nanoparticle.

The use of nanoparticles in organic materials has been greatly facilitated by the use of organic surfactant molecules that provide adequate passivation of the surface and solubility with the most common solvents. Since the first report on the use of nanoparticles as sensitizers in a polymeric system [173] the role of the surfactant in the electron-transfer reaction leading to charge generation has been a major topic of research. A general strategy to achieve efficient charge transfer has been outlined by considering electroactive surfactants that can mediate the electron-transfer between the transport agent and the nanocrystal by creating a CT complex with the nanoparticle that may lead to a physical separation of the electron and hole created upon optical excitation [174].

PVK doped with CdS nanoparticles (2 wt%) coated with *p*-thiocresol was first reported to display a larger photosensitivity than a composite comprising PVK/C_{60} (1 wt%) by Winiarz and coworkers [175]. A PVK/CdS (*p*-thiocresol)-based photorefractive polymer was reported shortly after with rather limited photorefractive properties with diffraction efficiencies $<5\,\%$ at fields as high as

140 V/μm, a two-beam coupling gain of 31 cm^{-1} at 107 V/μm and a response time of 7 s at 80 V/μm under a 0.5 W/cm^2 writing irradiance [17]. CdSe quantum dots surrounded by a CdSe shell and passivated by tri-*n*-octylphosphine oxide (TOPO) and CdSe passivated with TOPO were also studied and found to display limited photorefractive performance [152, 176]. In another study, CdSe nanoparticles capped with 4-methylbenzenethiol were used to dope a PVK-based photorefractive composite [153]. In this study the authors found greatly enhanced photoconductivity values (ca. 30 pS/cm at 70 V/μm) in the photorefractive polymer blend when compared with the values displayed by the photoconducting matrix PVK/ CdSe (4-methylbenzenethiol) (ca. 7 pS/cm at 70 V/μm). The enhanced photoconductive response was attributed to the formation of a CT complex between the CdSe nanoparticle and at least one of the chromophores used in the photorefractive composite, a blend of 3-(*N*,*N*-di-*n*-butylaniline-4-yl)-1-dicyanomethylidene-2cyclohexene (DBDC) or 4-homopiperidino-benzylidene-malononitrile (7DCST). Good photorefractive performance at 632 nm and fast response times ca. 100 ms were found in this polymer composite [153]. NiS nanocrystals capped with oleic acid or pyridine have also been used to dope a PVK-based photorefractive composite displaying photogeneration quantum efficiency values around 1 %, good photorefractive properties at 633 nm and response times ca. 500 ms [177].

In addition to reports in the visible range, the steady-state properties of photorefractive polymers based on PVK doped with PbS or HgS nanoparticles capped with *p*-thiocresol were reported at 1310 nm [178]. For the PbS sensitized material, photogeneration quantum efficiency values ca 0.1 % at 20 V/μm and gain coefficient values of 45 cm^{-1} at 52 V/μm were reported. In contrast, the HgS nanoparticle sensitized composite displayed photogeneration quantum efficiency values ca 2.5×10^{-4} % at 20 V/μm and a gain coefficient of 4.35 cm^{-1} at 90 V/μm. Nanoparticles of $LiNbO_3$, Cu_2S, and PbSe have also been studied as sensitizers of photorefractive polymers in the literature [179].

Very recently, a novel approach in the use of quantum dots as sensitizers was reported by Moon and coworkers wherein the photorefractive properties of a composite based on PVK doped with PbS nanocrystals capped with oleic acid or 1-octadecene were studied off-resonance, at 633 nm, instead of on-resonance, at 1220 nm (where PbS displays its first excitonic transition). Using this approach, the authors found that a photorefractive polymer doped with PbS at 4 wt.% displayed photoconductivity values up to 150 pS/cm at 80 V/μm, external diffraction efficiency ca. 50 %, two-beam-coupling gain coefficients of 211 cm^{-1}, and response times of 34 ms [180].

This none exhaustive review of photoconductors used in organic photorefractives reveals the need to develop novel strategies to enhance photogeneration, in order to rapidly generate, move, and trap the carriers needed to build the space-charge field, a process that favors the dynamic response of the photorefractive material; while on the other hand, the need for minimizing absorption losses in order to maximize the steady-state photorefractive performance, namely to maximize the external diffraction efficiency and the two-beam coupling net gain coefficient, both of which are

reduced by increased absorption. To overcome existing tradeoffs, significant improvements of the photoconductive properties of organic photorefractive materials need to be achieved. The following sections provide a general overview of current strategies pursued to optimize charge transport and photogeneration in state-of-the-art organic semiconductors.

2.10.2 Small-Molecule Semiconductors: Semicrystalline Materials and Molecular Glasses

Small-molecule materials commonly exhibit high mobility values due to the tendency to form extended crystalline phases as well as for the ease of purification compared to polymeric systems. High mobility small molecule materials display a low reorganization energy and high transfer integrals in addition to reduced number of impurities.

Advances in charge carrier mobility values have been remarkable over the last few years in the context of organic field effect transistor (OFETs) research. In addition to improved molecular design, some of the biggest breakthroughs have been related to improved control over the crystal growth and orientation using shearing techniques [6, 181], or guided crystallization on the liquid surface of an "antisolvent" droplet [182]. Molecular design motifs leading to high performing small-molecule donor materials include acenes and fused heteroacene, displaying maximum mobility values up to 11 cm^2/Vs [183]; benzothiophenes, such as 2,7-dioctyl[1]benzothieno[3,2-*b*][1]benzothiophene (BTBT) first reported to display average and maximum mobility values of 16 and 31 cm^2/Vs, respectively [182], and more recently shown capable of displaying average and maximum mobility values of 25 and 43 cm^2/Vs, respectively [6]. Other molecular motifs of promise include titanylphtalocyanine (TiOPc) and dithiophene-tetrathiafulvalene (TTF) displaying mobility values larger than 3 cm^2/Vs. A recent review of progress in OFET research can be found in [40] and references therein.

In the context of OPV, several classes of molecular donors have also been used. Recent reviews can be found in [184, 185] and references therein. Dyes, like phthalocyanine (Pc), subphthalo-cyanine (SubPc), merocyanine (MC), squaraine (SQ), diketo-pyrrolopyrroles (DPP), borondipyrromethene (BODIPY), isoindigo (IID), perylene diimides (PDIs), and quinacridone (QD), have been used in photovoltaic devices due to their large absorption coefficients. Such dyes have been shown to display mobility values in the range between 10^{-7} and 10^{-3} cm^2/Vs [184], measured by either space-charge limited current techniques (SCLC) or in an OFET configuration. Oligothiophenes and similar molecules have also been widely used in OPV research, leading to high power conversion efficiency (PCE) values of up to ca. 9.0 % [3]. Oligothiophenes display typical mobility values in the range between 10^{-4} and 10^{-1} cm^2/Vs [184], measured by SCLC or OFET techniques. Triphenylamine (TPA) has also been a common motif used in small-molecule donors for OPVs reaching PCE

up to around 6.4 % [186]. TPA-based donors typically display mobility values in the range between 10^{-6} and 10^{-4} cm^2/Vs [184], using SCLC or OFET techniques.

Fullerenes and their derivatives remain the most important class of acceptor materials for OPV applications [184]; however, recent advances in molecular acceptors for OFET research have started to attract increased attention to molecules based on other molecular motifs such as rylene diimides and PDIs, one of the most commonly used motifs in high performance acceptor materials for OFET and OPV applications.

Small molecule systems can also form amorphous glasses [185]. Amorphous molecular materials comprise molecules having non-planar geometries and bulky substituents, thus, characterized by the presence of free volume due to disorder in molecular orientations and positions. Polycrystalline small molecules have been most commonly used in OPV and OFET applications. In contrast, molecular glasses have been primarily studied in the context of organic light-emitting diodes (OLEDs). Typical motifs of molecular glasses include donor molecules such as tris(diphenylamino)-triphenylamine (TDATA), star-shaped compounds with a triphenylamine central core; tris(diphenyl-amino)benzene (TDAB), star-shaped compounds with a benzene central core; tris-(oligoarylenyl)amines; π-electron molecules capped with triarylamines; star-shaped molecules with a carbazone core; among many others [185]. Mobility values of these hole transporting amorphous glasses have been reported to be in the range between 10^{-6} and 10^{-2} cm^2/Vs; the latter, displayed by several tris(oligoarylenyl)amines. Acceptor molecules of interest include oxadiazole-containing oligo(arylene)s and oligo(arylenevinylene)s; compounds with a benzene or triazine central core; π-electron molecules capped with dimesitylboryl group; among many others. Mobility values of these electron transporting amorphous glasses are in the range between 10^{-6} and 10^{-4} cm^2/Vs [185].

Molecular glasses have also led to photorefractive glasses with attractive properties since the density of nonlinear optical moieties and transporting molecules can be maximized [127, 187–191]. Although photorefractive glasses had typically displayed slow response times, recently, Cao and coworkers reported on a bifunctional molecular glass comprising tetraphenyldiaminobiphenyl (TPD) as charge-transporting unit and 4-dicyanovinylaniline (DCVA) as an EO active unit that exhibits response times ca. 30 ms due to improved photoconductive properties [165].

2.10.3 Donor–Acceptor Polymers

Charge carrier mobility in amorphous polymers is known to be severely impaired by energetic and positional disorder. If strategies can be implemented to reduce energetic disorder, mobility values up to ca. 10^{-2} cm^2/Vs can be achieved [192]. On the other hand, it is also known that in semicrystalline polymers, wherein intermolecular packing leads to well-organized lamellar structures such as the

ones found in polyhexithiophene (P3HT) and poly(2,5-bis(3-alkylthiophen-2-yl) thieno(3,2-*b*)thiophene) (PBDTTT), charge mobility values up to ca. 1.0 cm^2/Vs can be achieved [193, 194].

In recent years, donor–acceptor copolymers have attracted the attention of the organic electronics community because they display unique and unexpected optical and electrical properties. Copolymers comprising donor and acceptor monomer repeat units were first proposed by Havinga and coworkers in 1992 as an approach towards designing materials with transparency in the visible spectral region and/or with large intrinsic conductivities [195, 196]. Alternation of donor and acceptor units in the backbone of these copolymers enable the formation of large intramolecular charge transfer complexes that increases intramolecular charge delocalization and results in low optical bandgaps. As we have described in the context of the use of sensitizers to increase the photoconductivity of photorefractive polymers, charge transfer complexes, arise when a donor with a small ionization potential and an acceptor with a large electron affinity electronically interact, leading to the formation of a new set of hybridized molecular orbitals with smaller fundamental energy gap than either constituent (Fig. 2.9). The electronic coupling and the geometric structure can be tailored by adjusting the relative strength of the donor and acceptor units. As a result, design rules can be developed to tune such factors as the ionization potential, electron affinity, optical gap, and transition dipole moments [197].

Since Havinga's seminal work, the increasing attention received by D–A copolymers to provide bandgap engineering in OPV and improve mobility values in both OFETs and OPVs has revealed some puzzling observations. For instance, Mühlbacher et al. first reported a low bandgap copolymer of cyclopentadithiophene and benzothiadiazole (PCPDTBT) that displayed ambipolar transport, with field-effect hole mobility values of. 2×10^{-2} cm^2/Vs and that resulted in OPVs displaying PCE values up to ca. 3.2 % [198] and later up to ca. 5.5 % [1]. Zhang and coworkers first reported a copolymer of cyclopentadithiophene and benzothiadiazole (CDT-BTZ) displaying hole mobility values around 0.17 cm^2/Vs in seemingly amorphous films [199]. The polycrystalline nature of CDT-BTZ was later confirmed, recently leading to the report of hole mobility values up to 5.5 cm^2/Vs in highly ordered polymer fibers [200], however, Yan and coworkers also reported a copolymer comprising naphthalenediimide (NDI) and bithiophene (PNDI2OD-T2) that displayed field-effect electron mobility values up to ca. 0.8 cm^2/Vs with high environmental stability [201]; balance ambipolar transport was also observed in BBTDPP1 a copolymer of diketopyrrolopyrrole (DPP) and thiophene with electron and hole mobility values ca. 0.1 cm^2/Vs and near-infrared emissive properties in polymer-light emitting diode and polymer light-emitting field-effect transistor configurations [8]. Copolymers of isoindigo (IID)- and indacenodithiophene with mobility values up to a value of 3.6 cm^2/Vs have been achieved [202]. Copolymers of indacenodithiophene and benzothiadiazole (IDT-BT) have also achieved mobility values around 3.6 cm^2/Vs in seemingly amorphous films [4, 203]. By no means, is this meant to be a comprehensive list of the most relevant observations and reports in *D–A* copolymers, but rather an illustration of the

remarkable properties achieved with materials that not only display comparable or better performance than semicrystalline polymers, but that more importantly, seem to defy existing design guidelines to achieve high mobility values through increased semicrystalline order.

Recent advances in rationalizing the intriguing properties of *D–A* copolymers seem to indicate that conjugate planes of the polymer exhibit a high degree of in-plane alignment of the polymer backbone due to its rigidity. This high degree of short range order is observed in both regions of a material displaying crystalline and non-crystalline order. The rigidity of the backbone thus seems to be crucial in enabling efficient intramolecular charge transport along the polymer backbone, requiring only occasional hopping through intermolecular π-stacking bridges to enable macroscopic charge transport [4, 38]. Noriega and coworkers [38] recently conducted a large survey on a set of semicrystalline, amorphous, and poorly ordered *D–A* copolymers that revealed that the activation energy of the mobility displayed by poorly ordered *D–A* copolymers is statistically indistinguishable from values displayed by semicrystalline polymers and much lower than values displayed by amorphous materials. To rationalize this observation, Noriega and co-authors argued that in classical semicrystalline polymers forming crystalline aggregates, the presence of disorder in the amorphous regions do not hinder charge transport as long as a percolating path remains for charge to move at macroscopic scales through a network of interconnecting aggregates. However, paracrystalline disorder in these materials is high and arises from fluctuations in the π–π stacking distances within the aggregates. Disorder in such a polymer hinders charge transport by introducing traps and manifest itself as an increased activation energy of the mobility. In contrast, aggregating *D–A* copolymers display poor microscopic order but a higher degree of paracrystallinity or short-range order than the one displayed by semicrystalline polymers. Short-range order is argued, enables efficient interchain charge transport within the aggregates but also efficient motion between aggregates along tie chains, thus providing a percolating network between aggregates that enables macroscopic charge transport, and at the same time, makes charge transport more tolerant of microscopic disorder.

As it should be clear from the material and discussions presented in this overview, exciting possibilities still exist both to improve our fundamental understanding of charge transport in state-of-the-art organic semiconductors and to improve the current performance of organic optoelectronic devices in general, and of photorefractive polymers in particular.

References

1. Peet, J., Kim, J.Y., Coates, N.E., Ma, W.L., Moses, D., Heeger, A.J., et al.: Efficiency enhancement in low-bandgap polymer solar cells by processing with alkane dithiols. Nat. Mater. **6**(7), 497–500 (2007)
2. Liu, Y., Zhao, J., Li, Z., Mu, C., Ma, W., Hu, H., et al.: Aggregation and morphology control enables multiple cases of high-efficiency polymer solar cells. Nat. Commun. **5**, 5293 (2014)

3. Zhang, Q., Kan, B., Liu, F., Long, G., Wan, X., Chen, X., et al.: Small-molecule solar cells with efficiency over 9%. Nat. Photon. **9**(1), 35–41 (2015)
4. Zhang, X., Bronstein, H., Kronemeijer, A.J., Smith, J., Kim, Y., Kline, R.J., et al.: Molecular origin of high field-effect mobility in an indacenodithiophene–benzothiadiazole copolymer. Nat. Commun. **4**, 2238 (2013)
5. Tseng, H.-R., Phan, H., Luo, C., Wang, M., Perez, L.A., Patel, S.N., et al.: High-mobility field-effect transistors fabricated with macroscopic aligned semiconducting polymers. Adv. Mater. **26**(19), 2993–2998 (2014)
6. Yuan, Y., Giri, G., Ayzner, A.L., Zoombelt, A.P., Mannsfeld, S.C.B., Chen, J., et al.: Ultra-high mobility transparent organic thin film transistors grown by an off-centre spin-coating method. Nat. Commun. **5**, 3005 (2014)
7. Venkateshvaran, D., Nikolka, M., Sadhanala, A., Lemaur, V., Zelazny, M., Kepa, M., et al.: Approaching disorder-free transport in high-mobility conjugated polymers. Nature **515**, 384–388 (2014)
8. Bürgi, L., Turbiez, M., Pfeiffer, R., Bienewald, F., Kirner, H.-J., Winnewisser, C.: High-mobility ambipolar near-infrared light-emitting polymer field-effect transistors. Adv. Mater. **20**(11), 2217–2224 (2008)
9. Gong, X., Tong, M., Xia, Y., Cai, W., Moon, J.S., Cao, Y., et al.: High-detectivity polymer photodetectors with spectral response from 300 nm to 1450 nm. Science **325**(5948), 1665–1667 (2009)
10. Armin, A., Hambsch, M., Kim, I.K., Burn, P.L., Meredith, P., Namdas, E.B.: Thick junction broadband organic photodiodes. Laser Photon. Rev. **8**(6), 924–932 (2014)
11. Armin, A., Jansen-van Vuuren, R.D., Kopidakis, N., Burn, P.L., Meredith, P.: Narrowband light detection via internal quantum efficiency manipulation of organic photodiodes. Nat. Commun. **6**, 6343 (2015)
12. Ashkin, A., Boyd, G.D., Dziedzic, J.M., Smith, R.G., Ballman, A.A., Levinstein, J.J., et al.: Optically-induced refractive index inhomogeneities in LiNbO3 and LiTaO3. Appl. Phys. Lett. **13**, 233 (1966)
13. Sutter, K., Gunter, P.: Photorefractive gratings in the organic crystal 2-cyclooctylamino-5-nitropyridine doped with 7,7,8,8-tetracyanoquinodimethane. J. Opt. Soc. Am. B **7**(12), 2274 (1990)
14. Sutter, K., Hullinger, J., Günter, P.: Photorefractive effects observed in the organic crystal 2-cyclooctylamino-5-nitropyridine doped with 7,7,8,8-tetracyanoquinodimethane. Solid State Commun. **74**(8), 867–870 (1990)
15. Ducharme, S., Scott, J.C., Twieg, R.J., Moerner, W.E.: Observation of the photorefractive effect in a polymer. Phys. Rev. Lett. **66**(14), 1846–1849 (1991)
16. Tamura, K., Padias, A.B., Hall Jr., H.K., Peyghambarian, N.: New polymeric material containing the tricyanovinylcarbazole group for photorefractive applications. Appl. Phys. Lett. **60**(15), 1803–1805 (1992)
17. Winiarz, J.G., Zhang, L.M., Lal, M., Friend, C.S., Prasad, P.N.: Observation of the photorefractive effect in a hybrid organic-inorganic nanocomposite. J. Am. Chem. Soc. **121** (22), 5287–5295 (1999)
18. Lundquist, P.M., Wortmann, R., Geletneky, C., Twieg, R.J., Jurich, M., Lee, V.Y., et al.: Organic glasses: a new class of photorefractive materials. Science **274**(5290), 1182–1185 (1996)
19. Khoo, I.C., Li, H., Liang, Y.: Observation of orientational photorefractive effects in nematic liquid crystals. Opt. Lett. **19**(21), 1723–1725 (1994)
20. Marder, S.R., Kippelen, B., Jen, A.K.Y., Peyghambarian, N.: Design and synthesis of chromophores and polymers for electro-optic and photorefractive applications. Nature (London) **388**, 845–851 (1997)
21. Kippelen, B., Meyers, F., Peyghambarian, N., Marder, S.R.: Chromophore design for photorefractive applications. J. Am. Chem. Soc. **119**(19), 4559–4560 (1997)
22. Meerholz, K., De Nardin, Y., Bittner, R.: Improved performance of photorefractive polymers based on merocyanine dyes in a polar matrix. Appl. Phys. Lett. **73**(1), 4–6 (1998)

23. Wright, D., Diaz-Garcia, M.A., Casperson, J.D., DeClue, M., Moerner, W.E., Twieg, R.J.: High-speed photorefractive polymer composites. Appl. Phys. Lett. **73**(11), 1490–1492 (1998)
24. Barzoukas, M., Blanchard-Desce, M.: Figures of merit of push-pull molecules in photorefractive polymers. J. Chem. Phys. **112**(4), 2036–2044 (2000)
25. Würthner, F., Wortmann, R., Meerholz, K.: Chromophore design for photorefractive organic materials. ChemPhysChem **3**, 17–31 (2002)
26. Herlocker, J.A., Ferrio, K.B., Hendrickx, E., Guenther, B.D., Mery, S., Kippelen, B., et al.: Direct observation of orientation limit in a fast photorefractive polymer composite. Appl. Phys. Lett. **74**(16), 2253–2255 (1999)
27. Van Steenwinckel, D., Hendrickx, E., Samyn, C., Engels, C., Persoons, A.: Effect of plasticizer and temperature on the photorefractive phase shift in fully functionalized polymethacrylates. J. Mater. Chem. **10**(12), 2692–2697 (2000)
28. Moerner, W.E., Silence, S.M., Hache, F., Bjorklund, G.C.: Orientationally enhanced photorefractive effect in polymers. J. Opt. Soc. Am. B **11**(2), 320 (1994)
29. Meerholz, K., Volodin, B.L., Sandalphon, Kippelen, B., Peyghambarian, N.: A photorefractive polymer with high optical gain and diffraction efficiency near 100%. Nature **371**(6497), 497–500 (1994)
30. Eralp, M., Thomas, J., Tay, S., Schulzgen, G.L.A., Norwood, R.A., Yamamoto, M., et al.: Submillisecond response of a photorefractive polymer under single nanosecond pulse exposure. Appl. Phys. Lett. **89**, 11 (2006)
31. Blanche, P.A., Bablumian, A., Voorakaranam, R., Christenson, C., Lin, W., Gu, T., et al.: Holographic three-dimensional telepresence using large-area photorefractive polymer. Nature **468**(7320), 80–83 (2010)
32. Tay, S., Blanche, P.-A., Voorakaranam, R., Tunc, A., Lin, W., Rokutanda, S., et al.: An updatable holographic three-dimensional display. Nature **451**(7179), 694–698 (2008)
33. Morrison, R.T.: Organic Chemistry, 5th edn. Allyn and Bacon, Boston (1987)
34. Ibach, H.: Solid-State Physics: An Introduction to Principles of Materials Science. Springer, Berlin (2010)
35. Kirchartz, T., Nelson, J.: Device modelling of organic bulk heterojunction solar cells. In: Beljonne, D., Cornil, J. (eds.) Multiscale Modelling of Organic and Hybrid Photovoltaics, vol. 352, pp. 279–324. Springer, Berlin (2014)
36. Brédas, J.L., Calbert, J.P., da Silva Filho, D.A., Cornil, J.: Organic semiconductors: a theoretical characterization of the basic parameters governing charge transport. Proc. Natl. Acad. Sci. **99**(9), 5804–5809 (2002)
37. Bredas, J.-L.: Mind the gap! Mater. Horiz. **1**(1), 17–19 (2014)
38. Noriega, R., Rivnay, J., Vandewal, K., Koch, F.P.V., Stingelin, N., Smith, P., et al.: A general relationship between disorder, aggregation and charge transport in conjugated polymers. Nat. Mater. **12**(11), 1038–1044 (2013)
39. Guillet, J.: Polymer Photophysics and Photochemistry: An Introduction to the Study of Photoprocesses in Macromolecules. Cambridge University Press, Cambridge (1985)
40. Sirringhaus, H.: 25th anniversary article: organic field-effect transistors: the path beyond amorphous silicon. Adv. Mater. **26**(9), 1319–1335 (2014)
41. Troisi, A.: Prediction of the absolute charge mobility of molecular semiconductors: the case of rubrene. Adv. Mater. **19**(15), 2000–2004 (2007)
42. Coropceanu, V., Cornil, J., da Silva Filho, D.A., Olivier, Y., Silbey, R., Brédas, J.-L.: Charge transport in organic semiconductors. Chem. Rev. **107**(4), 926–952 (2007)
43. Ashcroft, N.W.: Solid State Physics. Saunders College, Philadelphia (1976)
44. Kittel, C.: Introduction to Solid State Physics, 8th edn. Wiley, Hoboken (2005)
45. Kao, K.-C.: Dielectric Phenomena in Solids with Emphasis on Physical Concepts of Electronic Processes. Academic Press, Amsterdam (2004)
46. Bandyopadhyay, S.: Physics of Nanostructured Solid State Devices. Springer, New York (2012)
47. Lynn, B., Blanche, P.-A., Peyghambarian, N.: Photorefractive polymers for holography. J. Polym. Sci. B **52**(3), 193–231 (2014)
48. Köber, S., Salvador, M., Meerholz, K.: Organic photorefractive materials and applications. Adv. Mater. **23**(41), 4725–4763 (2011)

49. Anderson, P.W.: Model for the electronic structure of amorphous semiconductors. Phys. Rev. Lett. **34**(15), 953–955 (1975)
50. Belitz, D., Kirkpatrick, T.R.: The Anderson-Mott transition. Rev. Mod. Phys. **66**(2), 261–380 (1994)
51. Lu, G., Blakesley, J., Himmelberger, S., Pingel, P., Frisch, J., Lieberwirth, I., et al.: Moderate doping leads to high performance of semiconductor/insulator polymer blend transistors. Nat. Commun. **4**, 1588 (2013)
52. Hwang, D.K., Fuentes-Hernandez, C., Fenoll, M., Yun, M., Park, J., Shim, J.W., et al.: Systematic reliability study of top-gate p-and n-channel organic field-effect transistors. ACS Appl. Mater. Interfaces **6**, 3378–3386 (2014)
53. Lous, E.J., Blom, P.W.M., Molenkamp, L.W., de Leeuw, D.M.: Schottky contacts on a highly doped organic semiconductor. Phys. Rev. B **51**(23), 17251–17254 (1995)
54. Qi, Y., Sajoto, T., Kröger, M., Kandabarow, A.M., Park, W., Barlow, S., et al.: A molybdenum dithiolene complex as p-dopant for hole-transport materials: a multitechnique experimental and theoretical investigation. Chem. Mater. **22**(2), 524–531 (2009)
55. Guo, S., Kim, S.B., Mohapatra, S.K., Qi, Y., Sajoto, T., Kahn, A., et al.: n-Doping of organic electronic materials using air-stable organometallics. Adv. Mater. **24**(5), 699–703 (2012)
56. Lüssem, B., Riede, M., Leo, K.: Doping of organic semiconductors. Phys Status Solidi A **210** (1), 9–43 (2013)
57. Wellmann, P., Hofmann, M., Zeika, O., Werner, A., Birnstock, J., Meerheim, R., et al.: High-efficiency p-i-n organic light-emitting diodes with long lifetime. J. Soc. Inf..Display **13**(5), 393–397 (2005)
58. Gao, Z.Q., Mi, B.X., Xu, G.Z., Wan, Y.Q., Gong, M.L., Cheah, K.W., et al.: An organic p-type dopant with high thermal stability for an organic semiconductor. Chem. Commun. **1**, 117–119 (2008)
59. Olthof, S., Mehraeen, S., Mohapatra, S.K., Barlow, S., Coropceanu, V., Brédas, J.-L., et al.: Ultralow doping in organic semiconductors: evidence of trap filling. Phys. Rev. Lett. **109**(17), 176601 (2012)
60. Olthof, S., Singh, S., Mohapatra, S.K., Barlow, S., Marder, S.R., Kippelen, B., et al.: Passivation of trap states in unpurified and purified C60 and the influence on organic field-effect transistor performance. Appl. Phys. Lett. **101**(25), 253303 (2012)
61. Pingel, P., Neher, D.: Comprehensive picture of p-type doping of P3HT with the molecular acceptor F4TCNQ. Phys. Rev. B **87**(11), 115209 (2013)
62. Kim, G.H., Shao, L., Zhang, K., Pipe, K.P.: Engineered doping of organic semiconductors for enhanced thermoelectric efficiency. Nat. Mater. **12**(8), 719–723 (2013)
63. Kido, J., Matsumoto, T.: Bright organic electroluminescent devices having a metal-doped electron-injecting layer. Appl. Phys. Lett. **73**, 2866–2868 (1998)
64. Gao, W., Kahn, A.: Electrical doping: the impact on interfaces of π -conjugated molecular films. J. Phys. Condens. Matter **15**(38), S2757 (2003)
65. Abe, Y., Hasegawa, T., Takahashi, Y., Yamada, T., Tokura, Y.: Control of threshold voltage in pentacene thin-film transistors using carrier doping at the charge-transfer interface with organic acceptors. Appl. Phys. Lett. **87**(15), 153506 (2005)
66. Zhou, Y., Fuentes-Hernandez, C., Shim, J., Meyer, J., Giordano, A.J., Li, H., et al.: A universal method to produce low–work function electrodes for organic electronics. Science **336**(6079), 327–332 (2012)
67. Dai, A., Zhou, Y., Shu, A.L., Mohapatra, S.K., Wang, H., Fuentes-Hernandez, C., et al.: Enhanced charge-carrier injection and collection via lamination of doped polymer layers p-doped with a solution-processible molybdenum complex. Adv. Funct. Mater. **24**(15), 2197–2204 (2014)
68. Wetzelaer, G.A.H., Koster, L.J.A., Blom, P.W.M.: Validity of the Einstein relation in disordered organic semiconductors. Phys. Rev. Lett. **107**, 6 (2011)
69. Li, L., Lu, N., Liu, M., Bässler, H.: General Einstein relation model in disordered organic semiconductors under quasiequilibrium. Phys. Rev. B **90**(21), 214107 (2014)
70. Holstein, T.: Studies of polaron motion: part II. The "small" polaron. Ann. Phys. **8**(3), 343–389 (1959)

71. Holstein, T.: Studies of polaron motion: part I. The molecular-crystal model. Ann. Phys. **8**(3), 325–342 (1959)
72. Hannewald, K., Bobbert, P.A.: Ab initio theory of charge-carrier conduction in ultrapure organic crystals. Appl. Phys. Lett. **85**(9), 1535–1537 (2004)
73. Borsenberger, P.M., Magin, E.H., Van der Auweraer, M., De Schryver, F.C.: The role of disorder on charge transport in molecularly doped polymers and related materials. Phys. Status Solidi A **140**, 9–45 (1993)
74. Miller, A., Abrahams, E.: Impurity conduction at low concentrations. Phys. Rev. **120**(3), 745–755 (1960)
75. Frenkel, J.: On pre-breakdown phenomena in insulators and electronic semi-conductors. Phys. Rev. **54**, 647–648 (1938)
76. Schein, L.B., Peled, A., Glatz, D.: The electric field dependence of the mobility in molecularly doped polymers. J. Appl. Phys. **66**(2), 686–692 (1989)
77. Coehoorn, R., Bobbert, P.A.: Physics of Organic Semiconductors, 2nd completely new rev. edn. Wiley-VCH, Weinheim (2012)
78. Bässler, H.: Charge transport in molecularly doped polymers. Philos. Mag. B Phys. Condensed Matter Stat. Mech. Electron. Opt. Magn. Prop. **50**(3), 347–362 (1984)
79. Bässler, H.: Charge transport in disordered organic photoconductors—a Monte-Carlo simulation study. Phys. Status Solidi B **175**(1), 15–56 (1993)
80. Bässler, H.: Nondispersive and dispersive transport in random organic photoconductors. Mol. Cryst. Liq. Cryst. Sci. Technol. Sect. A **252**, 11–21 (1994)
81. Vanderauweraer, M., Deschryver, F.C., Borsenberger, P.M., Bassler, H.: Disorder in charge-transport in doped polymers. Adv. Mater. **6**(3), 199–213 (1994)
82. Goonesekera, A., Ducharme, S.: Effect of dipolar molecules on carrier mobilities in photorefractive polymer. J. Appl. Phys. **85**(9), 6506–6514 (1999)
83. Dieckmann, A., Bassler, H., Borsenberger, P.M.: An assessment of the role of dipoles on the density-of-states function of disordered molecular-solids. J. Chem. Phys. **99**(10), 8136–8141 (1993)
84. Young, R.H.: Dipolar lattice model of disorder in random media analytical evaluation of the Gaussian disorder model. Philos. Mag. Part B **72**(4), 435–457 (1995)
85. Hirao, A., Nishizawa, H.: Effect of dipoles on carrier drift and diffusion of molecularly doped polymers. Phys. Rev. B **56**(6), R2904–R2907 (1997)
86. Dunlap, D.H., Parris, P.E., Kenkre, V.M.: Charge-dipole model for the universal field dependence of mobilities in molecularly doped polymers. Phys. Rev. Lett. **77**(3), 542 (1996)
87. Maldonado, J.L., Bishop, M., Fuentes-Hernandez, C., Caron, P., Domercq, B., Zhang, Y.D., et al.: Effect of substitution on the hole mobility of bis(diarylamino)biphenyl derivatives doped in poly(styrene). Chem. Mater. **15**(4), 994–999 (2003)
88. Novikov, S.V., Dunlap, D.H., Kenkre, V.M., Parris, P.E., Vannikov, A.V.: Essential role of correlations in governing charge transport in disordered organic materials. Phys. Rev. Lett. **81**(20), 4472 (1998)
89. Fishchuk, I.I., Hertel, D., Bässler, H., Kadashchuk, A.K.: Effective-medium theory of hopping charge-carrier transport in weakly disordered organic solids. Phys. Rev. B **65**(12), 125201 (2002)
90. Fishchuk, I.I., Kadashchuk, A.K., Bassler, H., Weiss, D.S.: Nondispersive charge-carrier transport in disordered organic materials containing traps. Phys. Rev. B **66**, 20 (2002)
91. Arkhipov, V.I., Reynaert, J., Jin, Y.D., Heremans, P., Emelianova, E.V., Adriaenssens, G.J., et al.: The effect of deep traps on carrier hopping in disordered organic materials. Synth. Met. **138**(1–2), 209–212 (2003)
92. Parris, P.E., Kenkre, V.M., Dunlap, D.H.: Nature of charge carriers in disordered molecular solids: are polarons compatible with observations? Phys. Rev. Lett. **87**(12), 126601 (2001)
93. Fishchuk, I.I., Kadashchuk, A., Bassler, H., Nespurek, S.: Nondispersive polaron transport in disordered organic solids. Phys. Rev. B **67**, 22 (2003)
94. Sirringhaus, H., Tessler, N., Friend, R.H.: Integrated optoelectronic devices based on conjugated polymers. Science **280**(5370), 1741–1744 (1998)

95. Salleo, A., Chen, T.W., Völkel, A.R., Wu, Y., Liu, P., Ong, B.S., et al.: Intrinsic hole mobility and trapping in a regioregular poly(thiophene). Phys. Rev. B **70**(11), 115311 (2004)
96. Coehoorn, R., Pasveer, W.F., Bobbert, P.A., Michels, M.A.J.: Charge-carrier concentration dependence of the hopping mobility in organic materials with Gaussian disorder. Phys. Rev. B **72**(15), 155206 (2005)
97. Coehoorn, R.: Hopping mobility of charge carriers in disordered organic host-guest systems: dependence on the charge-carrier concentration. Phys. Rev. B **75**(15), 155203 (2007)
98. Pasveer, W.F., Cottaar, J., Tanase, C., Coehoorn, R., Bobbert, P.A., Blom, P.W.M., et al.: Unified description of charge-carrier mobilities in disordered semiconducting polymers. Phys. Rev. Lett. **94**(20), 206601–206604 (2005)
99. Zhou, J., Zhou, Y.C., Zhao, J.M., Wu, C.Q., Ding, X.M., Hou, X.Y.: Carrier density dependence of mobility in organic solids: a Monte Carlo simulation. Phys. Rev. B **75**(15), 153201 (2007)
100. Bässler, H., Köhler, A.: Charge transport in organic semiconductors. In: Metzger, R.M. (ed.) Unimolecular and supramolecular electronics I, vol. 312, pp. 1–65. Springer, Berlin (2012)
101. Herlocker, J.A., Fuentes-Hernandez, C., Ferrio, K.B., Hendrickx, E., Blanche, P.A., Peyghambarian, N., et al.: Stabilization of the response time in photorefractive polymers. Appl. Phys. Lett. **77**(15), 2292–2294 (2000)
102. Ostroverkhova, O., Singer, K.D.: Space-charge dynamics in photorefractive polymers. J. Appl. Phys. **92**(4), 1727–1743 (2002)
103. Fuentes-Hernandez, C., Thomas, J., Termine, R., Meredith, G., Peyghambarian, N., Kippelen, B., et al.: Video-rate compatible photorefractive polymers with stable dynamic properties under continuous operation. Appl. Phys. Lett. **85**(11), 1877–1879 (2004)
104. Thomas, J., Fuentes-Hernandez, C., Yamamoto, M., Cammack, K., Matsumoto, K., Walker, G.A., et al.: Bistriarylamine polymer-based composites for photorefractive applications. Adv. Mater. **16**(22), 2032–2036 (2004)
105. Mecher, E., Gallego-G¢mez, F., Tillmann, H., Horhold, H.-H., Hummelen, J. C., Meerholz, K.: Near-infrared sensitivity enhancement of photorefractive polymer composites by pre-illumination. Nature **418**, 959–964 (2002).
106. Kulikovsky, L., Neher, D., Mecher, E., Meerholz, K., Horhold, H.H., Ostroverkhova, O.: Photocurrent dynamics in a poly(phenylene vinylene)-based photorefractive composite. Phys. Rev. B **69**, 125216-1–125216-11 (2004)
107. Mecher, E., Gallego-Gomez, F., Meerholz, K., Tillmann, H., Horhold, H.H., Hummelen, J.C.: Photophysical and redox NIR-sensitivity enhancement in photorefractive polymer composites. ChemPhysChem **5**(2), 277–284 (2004)
108. Kippelen, B., Blanche, P.A., Schulzgen, A., Fuentes-Hernandez, C., Ramos-Ortiz, G., Wang, J.F., et al.: Photorefractive polymers with non-destructive readout. Adv. Funct. Mater. **12**(9), 615–620 (2002)
109. Blanche, P.A., Kippelen, B., Schulzgen, A., Fuentes-Hernandez, C., Ramos-Ortiz, G., Wang, J.F., et al.: Photorefractive polymers sensitized by two-photon absorption. Opt. Lett. **27**(1), 19–21 (2002)
110. Tay, S., Thomas, J., Eralp, M., Li, G.Q., Kippelen, B., Marder, S.R., et al.: Photorefractive polymer composite operating at the optical communication wavelength of 1550 nm. Appl. Phys. Lett. **85**(20), 4561–4563 (2004)
111. Tay, S., Thomas, J., Eralp, M., Li, G.Q., Norwood, R.A., Schulzgen, A., et al.: High-performance photorefractive polymer operating at 1550 nm with near-video-rate response time. Appl. Phys. Lett. **87**, 17 (2005)
112. Nolt, D.D. (ed.): Photorefractive effects and materials. Kluwer, Boston (1995).
113. Hendrickx, E., Zhang, Y., Ferrio, K.B., Herlocker, J.A., Anderson, J., Armstrong, N.R., et al.: Photoconductive properties of PVK-based photorefractive polymer composites doped with fluorinated stryrene chromophores. J. Mater. Chem. **9**, 2251–2258 (1999)

114. Däubler, T.K., Bittner, R., Meerholz, K., Cimrov, V., Neher, D.: Charge carrier photogeneration, trapping, and space-charge field formation in PVK-based photorefractive materials. Phys. Rev. B **61**(20), 13515–13527 (2000)
115. Nespurek, S., Cimrova, V., Pfleger, J., Kminek, I.: Free charge carrier formation in polymers under illumination. Polym. Adv. Technol. **7**(5–6), 459–470 (1996)
116. Davidenko, N.A., Zabolotnyi, M.A., Ishchenko, A.A., Kuvshinskii, N.G., Borolina, N.P.: Electric field effects on photoconductivity and electronic absorption spectra of photogeneration sites in amorphous molecular semiconductors. High Energy Chem. **38**(1), 13–20 (2004)
117. Onsager, L.: Initial recombination of ions. Phys. Rev. **54**, 554–557 (1938)
118. Islam, M.A.: Einstein–Smoluchowski diffusion equation: a discussion. Phys. Scr. **70**(2–3), 120 (2004)
119. Mozumder, A.: Effect of an external electric field on the yield of free ions. 1. General results from the Onsager theory. J. Chem. Phys. **60**(11), 4300–4304 (1974)
120. Braun, L.C.: Electric field assisted dissociation of charge transfer states as a mechanism of photocarrier production. J. Chem. Phys. **80**(9), 4157–4161 (1984)
121. Noolandi, J., Hong, K.M.: Theory of photogeneration and fluorescence quenching. J. Chem. Phys. **70**(7), 3230–3236 (1979)
122. Marcus, R.A., Siders, P.: Theory of highly exothermic electron-transfer reactions. J. Phys. Chem. **86**(5), 622–630 (1982)
123. Marcus, R.A.: Electron-transfer reactions in chemistry—theory and experiment. Rev. Mod. Phys. **65**(3), 599–610 (1993)
124. Wang, Y., Suna, A.: Fullerenes in photoconductive polymers. Charge generation and charge transport. J. Phys. Chem. B **101**(29), 5627–5638 (1997)
125. Schildkraut, J.S., Buettner, A.V.: Theory and simulation of the formation and erasure of space-charge gratings in photoconductive polymers. J. Appl. Phys. **72**(5), 1888–1893 (1992)
126. Schildkraut, J.S., Cui, Y.: Zero-order and first-order theory of the formation of space-charge gratings in photoconductive polymers. J. Appl. Phys. **72**(11), 5055–5060 (1992)
127. Ostroverkhova, O., Moerner, W.E.: Organic photorefractives: mechanisms, materials, and applications. Chem. Rev. **104**(7), 3267–3314 (2004)
128. Langevin, P.: Recombinaison et mobilites des ions dans les gaz. Ann. Chim. Phys **28**, 433 (1903)
129. Silver, M., Sharma, R.: Carrier generation and recombination in anthracene. J. Chem. Phys. **46**(2), 692–696 (1967)
130. Albrecht, U., Bassler, H.: Langevin-type charge-carrier recombination in a disordered hopping system. Phys. Status Solidi B **191**(2), 455–459 (1995)
131. Nenashev, A.V., Jansson, F., Baranovskii, S.D., Österbacka, R., Dvurechenskii, A.V., Gebhard, F.: Role of diffusion in two-dimensional bimolecular recombination. Appl. Phys. Lett. **96**(21), 213304 (2010)
132. Greenham, N.C., Bobbert, P.A.: Two-dimensional electron-hole capture in a disordered hopping system. Phys. Rev. B **68**(24), 245301 (2003)
133. Adriaenssens, G.J., Arkhipov, V.I.: Non-Langevin recombination in disordered materials with random potential distributions. Solid State Commun. **103**(9), 541–543 (1997)
134. Nelson, J.: Diffusion-limited recombination in polymer-fullerene blends and its influence on photocurrent collection. Phys. Rev. B **67**(15), 155209 (2003)
135. Kukhtarev, N.V., Markov, V.B., Odulov, S.G., Soskin, M.S., Vinetskii, V.L.: Holographic storage in electrooptic crystals. 1. Steady-state. Ferroelectrics **22**(3–4), 949–960 (1979)
136. Kukhtarev, N.V., Markov, V.B., Odulov, S.G., Soskin, M.S., Vinetskii, V.L.: Holographic storage in electrooptic crystals. 2. Beam coupling-light amplification. Ferroelectrics **22**(3–4), 961–964 (1979)
137. Fuentes-Hernandez, C., Thomas, J., Meredith, G.R., Peyghambarian, N.N., Marder, S.R., Kippelen, B.: Trapping mechanisms and dynamics in bis-triarylamine-based photorefractive polymer composites. In: Organic Holographic Materials and Applications II, Denver, CO, USA, pp. 96–102 (2004).

138. Cui, Y., Swedek, B., Cheng, N., Zieba, J., Prasad, P.N.: Dynamics of photorefractive grating erasure in polymeric composites. J. Appl. Phys. **85**(1), 38–43 (1999)
139. Yuan, B., Sun, X., Hou, C., Li, Y., Zhou, Z., Jiang, Y., et al.: Kinetics of the formation of space-charge field in photorefractive polymers. J. Appl. Phys. **88**(10), 5562–5569 (2000)
140. Yuan, B., Sun, X., Jiang, Y., Hou, C., Zhou, Z.: Effect of the applied electric field on the steady state and temporary state space-charge field in photorefractive polymers. J. Modern Opt. **48**(7), 1161–1170 (2001)
141. Yuan, B., Sun, X., Zhou, Z., Li, Y., Jiang, Y., Hou, C.: Theory of space-charge field with a moving fringe in photorefractive polymers. J. Appl. Phys. **89**(11), 5881–5888 (2001)
142. Yuan, B.H., Sun, X.D., Jiang, Y.Y., Zhou, Z.X., Hou, C.F., Li, Y.: Comparisons between two models of the formation of space charge field in photorefractive polymers. Phys. Lett. A **292** (6), 338–348 (2002)
143. Grunnet-Jepsen, A., Wright, D., Smith, B., Bratcher, M.S., DeClue, M.S., Siegel, J.S., et al.: Spectroscopic determination of trap density in C 60-sensitized photorefractive polymers. Chem. Phys. Lett. **291**, 553–561 (1998)
144. Grunnet-Jepsen, A., Thompson, C.L., Twieg, R.J., Moerner, W.E.: High performance photorefractive polymers with improved stability. Appl. Phys. Lett. **70**(12), 1515–1517 (1997)
145. Grunnet-Jepsen, A., Thompson, C.L., Twieg, R.J., Moerner, W.E.: Amplified scattering in a high-gain photorefractive polymer. J. Opt. Soc. Am. B **15**(2), 901–904 (1998)
146. Meerholz, K., Mecher, E., Bittner, R., De Nardin, Y.: Competing photorefractive gratings in organic thin-film devices. J. Opt. Soc. Am. B **15**(7), 2114–2124 (1998)
147. Binks, D.J., Khand, K., West, D.P.: Reorientation of chromophores in dispersive photorefractive polymers. J. Opt. Soc. Am. B **18**(3), 308–312 (2001)
148. Zhang, Y., Cui, Y., Prasad, P.N.: Observation of photorefractivity in a fullerene-doped polymer composite. Phys. Rev. B **46**(15), 9900–9902 (1992)
149. Moon, I.K., Choi, J., Kim, N.: High-performance photorefractive composite based on non-conjugated main-chain, hole-transporting polymer. Macromol. Chem. Phys. **214**(4), 478–485 (2013)
150. Peng, Z., Gharavi, A.R., Yu, L.: Synthesis and characterization of photorefractive polymers containing transition metal complexes as photosensitizer. J. Am. Chem. Soc. **119**(20), 4622–4632 (1997)
151. Aiello, I., Dattilo, D., Ghedini, M., Bruno, A., Termine, R., Golemme, A.: Cyclopalladated complexes as photorefractive materials with high refractive index modulation. Adv. Mater. **14**(17), 1233–1236 (2002)
152. Binks, D.J., Bant, S.P., West, D.P., O'Brien, P., Malik, M.A.: CdSe/CdS core/shell quantum dots as sensitizer of a photorefractive polymer composite. J. Modern Opt. **50**(2), 299–310 (2003)
153. Fuentes-Hernandez, C., Suh, D.J., Kippelen, B., Marder, S.R.: High-performance photorefractive polymers sensitized by cadmium selenide nanoparticles. Appl. Phys. Lett. **85**(4), 534–536 (2004)
154. Hendrickx, E., Kippelen, B., Thayumanavan, S., Marder, S.R., Persoons, A., Peyghambarian, N.: High photogeneration efficiency of charge-transfer complexes formed between low ionization potential arylamines and C60. J. Chem. Phys. **112**(21), 9557–9561 (2000)
155. Wang, Y.: Photoconductivity of fullerene-doped polymers. Nature **356**(6370), 585–587 (1992)
156. Silence, S.M., Donckers, J.M., Walsh, C.A., Twieg, R.J., Moerner, W.E.: Optical properties of poly (N-vynilcarbazole)-based guest-host photorefractive polymer systems. Appl. Optics **33**(11), 2218–2222 (1994)
157. Ogino, K., Nomura, T., Shichi, T., Park, S.-H., Sato, H.: Synthesis of polymers having tetraphenyldiaminobiphenyl units for a host polymer of photorefractive composite. Chem. Mater. **9**, 2768–2775 (1997)
158. Zhang, Y.D., Wada, T., Sasabe, H.: Carbazole photorefractive materials. J. Mater. Chem. **8** (4), 809–828 (1998)
159. Bolink, H.J., Arts, C., Krasnikov, V.V., Malliaras, G.G., Hadziioannou, G.: Novel bifunctional molecule for photorefractive materials. Chem. Mater. **9**(6), 1407–1413 (1997)

160. Eralp, M., Thomas, J., Tay, S., Li, G., Meredith, G., Schulzgen, A., et al.: High-performance photorefractive polymer operating at 975 nm. Appl. Phys. Lett. **85**(7), 1095–1097 (2004)
161. Tsutsumi, N., Kinashi, K., Masumura, K., Kono, K.: Photorefractive performance of poly (triarylamine)-based polymer composites: an approach from the photoconductive properties. J. Polym. Sci. B **53**(7), 502–508 (2015)
162. Hofmann, U., Grasruck, M., Schreiber, A., Schloter, S., Hohle, C., Strohriegl, P., et al.: Correlation between dispersivity of charge transport and holographic response time in organic photorefractive glass. J. Phys. Chem. B **104**, 3887–3891 (2000)
163. Redecker, M., Bradley, D.D.C., Inbasekaran, M., Wu, W.W., Woo, E.P.: High mobility hole transport fluorene-triarylamine copolymers. Adv. Mater. **11**(3), 241–246 (1999)
164. Hofmann, U., Schreiber, A., Haarer, D., Zilker, S.J., Bacher, A., Bradley, D.D.C., et al.: Investigations on the grating dynamics in a fast photorefractive guest–host polymer. Chem. Phys. Lett. **311**(1–2), 41–46 (1999)
165. Cao, Z., Tsuchiya, K., Ogino, K.: Fast photorefractive response in triphenylamine-based molecular glass. Chem. Lett. **41**(11), 1541–1543 (2012)
166. Grishina, A.D., Krivenko, T.V., Savel'ev, V.V., Rychwalski, R.W., Vannikov, A.V.: Photoelectric, nonlinear optical, and photorefractive properties of polyvinylcarbazole composites with graphene. High Energy Chem. **47**(2), 46–52 (2013)
167. Vannikov, A.V., Rychwalski, R.W., Grishina, A.D., Pereshivko, L.Y., Krivenko, T.V., Savel'ev, V.V., et al.: Photorefractive polymer composites for the IR region based on carbon nanotubes. Opt. Spectrosc. **99**(4), 643–648 (2005)
168. Lingam, N.K., Kalghatgi, S., Winiarz, J.G.: Enhanced photorefractivity in a polymeric composite photosensitized with carbon nanotubes grafted to a photoconductive polymer. J. Appl. Phys. **109**(2), 023106 (2011)
169. Chantharasupawong, P., Christenson, C.W., Philip, R., Zhai, L., Winiarz, J., Yamamoto, M., et al.: Photorefractive performances of a graphene-doped PATPD/7-DCST/ECZ composite. J. Mater. Chem. C **2**(36), 7639–7647 (2014)
170. Gallego-Gómez, F., Quintana, J.A., Villalvilla, J.M., Díaz-García, M.A., Martín-Gomis, L., Fernández-Lázaro, F., et al.: Phthalocyanines as efficient sensitizers in low-Tg hole-conducting photorefractive polymer composites. Chem. Mater. **21**(13), 2714–2720 (2009)
171. Köber, S., Prauzner, J., Salvador, M., Kooistra, F.B., Hummelen, J.C., Meerholz, K.: 1064-nm sensitive organic photorefractive composites. Adv. Mater. **22**(12), 1383–1386 (2010)
172. Alivisatos, A.P.: Semiconductor clusters, nanocrystals, and quantum dots. Science **271** (5251), 933–937 (1996)
173. Wang, Y., Herron, N.: Photoconductivity of CdS nanocluster-doped polymers. Chem. Phys. Lett. **200**(1–2), 71–75 (1992)
174. Milliron, D.J., Alivisatos, A.P., Pitois, C., Edder, C., Fréchet, J.M.J.: Electroactive surfactant designed to mediate electron transfer between CdSe Nanocrystals and organic semiconductors. Adv. Mater. **15**(1), 58–61 (2003)
175. Winiarz, J.G., Zhang, L.M., Lal, M., Friend, C.S., Prasad, P.N.: Photogeneration, charge transport, and photoconductivity of a novel PVK/CdS-nanocrystal polymer composite. Chem. Phys. **245**(1–3), 417–428 (1999)
176. Binks, D.J., West, D.P., Norager, S., O'Brien, P.: Field-independent grating formation rate in a photorefractive polymer composite sensitized by CdSe quantum dots. J. Chem. Phys. **117** (15), 7335–7341 (2002)
177. Fears, T.M., Anderson, C., Winiarz, J.G.: Photorefractivity in a polymeric composite photosensitized with NiS nanocrystals. J. Chem. Phys. **129**, 15 (2008)
178. Winiarz, J.G., Zhang, L., Park, J., Prasad, P.N.: Inorganic: organic hybrid nanocomposites for photorefractivity at communication wavelengths. J. Phys. Chem. B **106**(5), 967–970 (2002)
179. Aslam, F., Stevenson-Hill, J., Binks, D.J., Daniels, S., Pickett, N.L., O'Brien, P.: Effect of nanoparticle composition on the performance of photorefractive polymers. Chem. Phys. **334** (1–3), 45–52 (2007)

180. Moon, J.-S., Liang, Y., Stevens, T.E., Monson, T.C., Huber, D.L., Mahala, B.D., et al.: Off-resonance photosensitization of a photorefractive polymer composite using PbS nanocrystals. J. Phys. Chem. C **119**(24), 13827–13835 (2015)
181. Giri, G., Verploegen, E., Mannsfeld, S.C.B., Atahan-Evrenk, S., Kim, D.H., Lee, S.Y., et al.: Tuning charge transport in solution-sheared organic semiconductors using lattice strain. Nature **480**(7378), 504–508 (2011)
182. Minemawari, H., Yamada, T., Matsui, H., Tsutsumi, J., Haas, S., Chiba, R., et al.: Inkjet printing of single-crystal films. Nature **475**(7356), 364–367 (2011)
183. Diao, Y., Tee, B.C.K., Giri, G., Xu, J., Kim, D.H., Becerril, H.A., et al.: Solution coating of large-area organic semiconductor thin films with aligned single-crystalline domains. Nat. Mater. **12**(7), 665–671 (2013)
184. Lin, Y., Li, Y., Zhan, X.: Small molecule semiconductors for high-efficiency organic photovoltaics. Chem. Soc. Rev. **41**(11), 4245–4272 (2012)
185. Shirota, Y., Kageyama, H.: Charge carrier transporting molecular materials and their applications in devices. Chem. Rev. **107**(4), 953–1010 (2007)
186. Chiu, S.-W., Lin, L.-Y., Lin, H.-W., Chen, Y.-H., Huang, Z.-Y., Lin, Y.-T., et al.: A donor-acceptor-acceptor molecule for vacuum-processed organic solar cells with a power conversion efficiency of 6.4%. Chem. Commun. **48**(13), 1857–1859 (2012)
187. Wang, L., Ng, M.-K., Yu, L.: Efficient molecular photorefractive materials based on methine dyes. Appl. Phys. Lett. **78**(6), 700–702 (2001)
188. Ostroverkhova, O., Wright, D., Gubler, U., Moerner, W.E., He, M., Sastre-Santos, A., et al.: Recent advances in understanding and development of photorefractive polymers and glasses. Adv. Funct. Mater. **12**(9), 621–629 (2002)
189. Ostroverkhova, O., He, M., Twieg, R.J., Moerner, W.E.: Role of temperature in controlling performance of photorefractive organic glasses. ChemPhysChem **4**(7), 732–744 (2003)
190. Choi, C.-S., Moon, I.K., Kim, N.: High-performance photorefractive organic glass based on diphenylhydrazone. Appl. Phys. Lett. **94**(5), 053302 (2009)
191. Zhang, L., Xu, S., Yang, Z., Cao, S.: Photorefractive effect in triphenylamine-based monolithic molecular glasses with low Tg. Mater. Chem. Phys. **126**(3), 804–810 (2011)
192. Veres, J., Ogier, S.D., Leeming, S.W., Cupertino, D.C., Mohialdin Khaffaf, S.: Low-k Insulators as the choice of dielectrics in organic field-effect transistors. Adv. Funct. Mater. **13**(3), 199–204 (2003)
193. McCulloch, I., Heeney, M., Bailey, C., Genevicius, K., MacDonald, I., Shkunov, M., et al.: Liquid-crystalline semiconducting polymers with high charge-carrier mobility. Nat. Mater. **5**(4), 328–333 (2006)
194. Hamadani, B.H., Gundlach, D.J., McCulloch, I., Heeney, M.: Undoped polythiophene field-effect transistors with mobility of 1cm2V-1s-1. Appl. Phys. Lett. **91**(24), 243512 (2007)
195. Havinga, E.E., ten Hoeve, W., Wynberg, H.: A new class of small band gap organic polymer conductors. Polym. Bull. **29**(1–2), 119–126 (1992)
196. Havinga, E.E., ten Hoeve, W., Wynberg, H.: Alternate donor-acceptor small-band-gap semiconducting polymers; polysquaraines and polycroconaines. Synth. Met. **55**(1), 299–306 (1993)
197. Pandey, L., Risko, C., Norton, J.E., Brédas, J.-L.: Donor–acceptor copolymers of relevance for organic photovoltaics: a theoretical investigation of the impact of chemical structure modifications on the electronic and optical properties. Macromolecules **45**(16), 6405–6414 (2012)
198. Mühlbacher, D., Scharber, M., Morana, M., Zhu, Z., Waller, D., Gaudiana, R., et al.: High photovoltaic performance of a low-bandgap polymer. Adv. Mater. **18**(21), 2884–2889 (2006)
199. Zhang, M., Tsao, H.N., Pisula, W., Yang, C., Mishra, A.K., Müllen, K.: Field-effect transistors based on a benzothiadiazole–cyclopentadithiophene copolymer. J. Am. Chem. Soc. **129**(12), 3472–3473 (2007)

200. Wang, S., Kappl, M., Liebewirth, I., Müller, M., Kirchhoff, K., Pisula, W., et al.: Organic field-effect transistors based on highly ordered single polymer fibers. Adv. Mater. **24**(3), 417–420 (2012)
201. Yan, H., Chen, Z., Zheng, Y., Newman, C., Quinn, J.R., Dotz, F., et al.: A high-mobility electron-transporting polymer for printed transistors. Nature **457**(7230), 679–686 (2009)
202. Lei, T., Dou, J.-H., Pei, J.: Influence of alkyl chain branching positions on the hole mobilities of polymer thin-film transistors. Adv. Mater. **24**(48), 6457–6461 (2012)
203. Zhang, W., Smith, J., Watkins, S.E., Gysel, R., McGehee, M., Salleo, A., et al.: Indacenodithiophene semiconducting polymers for high-performance, air-stable transistors. J. Am. Chem. Soc. **132**(33), 11437–11439 (2010)

http://www.springer.com/978-3-319-29332-5

Photorefractive Organic Materials and Applications
Blanche, P.-A. (Ed.)
2016, X, 318 p. 162 illus., 62 illus. in color., Hardcover
ISBN: 978-3-319-29332-5